Transport Upscaling in Porous Media

Master of Science Thesis
Renewable Energy

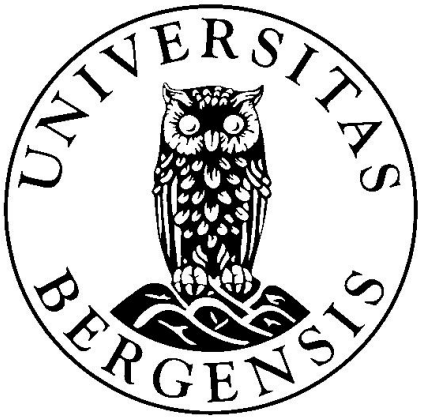

Anette Nedreli

Department of Geophysics
University of Bergen

June 2, 2014

Acknowledgments

First of all I would like to thank my supervisors Eirik Keilegavlen and Inga Berre for all their help and support. Their enthusiasm and guidance has been indispensable, and I'm really grateful for their time, inspiration and explanations, it really helped me a lot. I would also like to thank Anna who has been to some of our supervisor meetings. Next, I would thank my friends and fellow students, especially the ones in the writing group. Also, I would like to thank my colleges at work for backing me up and supporting my thesis. Lastly, I would like to give a special thank my family including my boyfriend for all their support, patience and care, and for cheering me up whenever needed.

Abstract

Numerical models are important for modeling what happens in porous media. In this thesis we will simulate the heat transport in geothermal reservoirs. Because these reservoirs are usually quite large, we will make a model that upgrids the fine scale reservoir into a coarser scale reservoir that has a smaller amount of grid cells. We will look at upgridding based on different indicators; Cartesian, permeability, velocity and time of flight. We need to upscale the energy equation so we can solve it in regards to temperature on the coarse grid. We will investigate what happens when we have a convection dominated heat transport, a diffusion dominated heat transport, and also what happens in between when we have a mix of both.

List of symbols

Here are the symbols used in this paper, along with a short explanation and their units.

Symbol	Explanation	Unit
A	Area	m^2
α	Half transmissibility	
c	Specific heat capacity	$J/\left(kg \cdot K\right)$
$\mathbf{g}$	Gravity	m/s^2
$\mathbf{k}$	Thermal conductivity	$W/\left(m \cdot K\right)$
$\mathbf{K}$	Permeability	$m^2,\ D$
L	Length	m
m	Mass	kg
μ	Viscosity	$kg/\left(m \cdot s\right)$
$\mathbf{n}$	Unit normal vector	$-$
Ω	Domain	
$\mathbf{p}$	Pressure	Pa
Pe	Péclet number	$-$
ϕ	Effective porosity	$-$
$\mathbf{q}$	Heat flux	W/m^2
Q	Net mass/heat production	$kg/\left(s \cdot m^3\right),\ W/\left(s \cdot m^3\right)$
ρ	Density	kg/m^3
S	Boundary of domain	
t	Time	s
t_{12}	Transmissibility	
T	Temperature	K
$\mathbf{v}$	Velocity	m/s
V	Volume	m^3

Contents

Chapter 1

Introduction

In this thesis we will use numerical solvers to simulate the heat transport in a geothermal reservoir. In this chapter we will first discuss a bit about the energy sources in the world before we give a brief description about what geothermal energy is all about. Then we will discuss a bit why we need numerical methods in a geothermal context. The introduction chapter is based on the sources [5] and [3].

In Chapter 2 we will present the equations we need to calculate the heat transport in our reservoir. Chapter 3 is about the numerical methods we use to solve the equations we found in Chapter 2. In Chapter 4 we will look at upscaling and upgridding of our reservoir grid. Finally, in Chapter 5 we use these methods on homogeneous and heterogeneous reservoirs to simulate the heat transport for different thermal conductivities, and explore how our upscaling method works.

1.1 Sources of energy

In the rich parts of the world we are used to having a lot of energy available to us in the forms of electricity, heat, light, fuel and more. Without energy, we could not use everyday utilities such as phones, computers, cars, ovens, lamps etc. In the poor parts of the world they do not have much of the luxury that energy gives. With the increasing use of energy by the poor people who raise out of poverty, and the rich people who continue to use more and more energy we get a growing demand for energy in the world. As we can see in Figure 1.1, the energy supply has more than doubled from 6 109 Mtoe in 1973 to 13 113 Mtoe in 2011, and it will continue to increase in the future.

We can divide the energy sources into renewable and non-renewable resources. Like the name suggests, renewable energy resources are renewed on a short timescale, while non-renewable resources are practically not renewed. Most of the energy is produced from non-renewable resources, such as coal, oil, and natural gas. These non-renewable resources

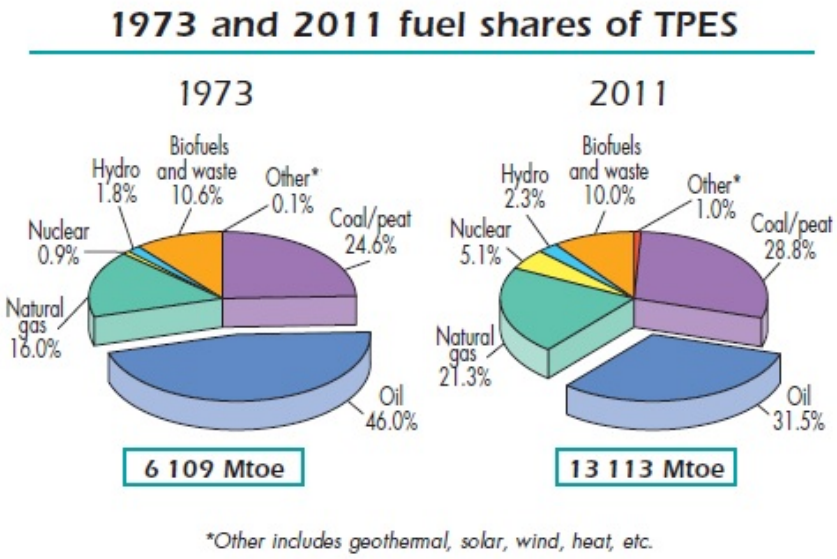

Figure 1.1: The total primary energy supply (TPES) sources in 1973 and 2011 for the world [3].

are called fossil fuels. These resources accounted for 86.7 % of the total energy supply in 2011 as we can see in Figure 1.1. Because these resources are nonrenewable they will eventually no longer be economical to produce, since the resources are getting scarcer and no longer profitable to extract. We might find new reserves that were previously unknown, so the total reserves are higher than the known reserves. We currently have enough of these non-renewable resources for several hundred years with the current production and growth rates, especially of coal. Another problem with the fossil fuel resources is that they release CO_2 and other gases into the atmosphere, where the gases will trap heat, which leads to global warming by the greenhouse effect. There will also be pollutants released, which can decrease life span of humans and other animals, and reduce life quality. Sometimes the fossil fuel extraction makes big nature disruption, for example by open pit mining, or when whole mountain tops are removed to collect for instance coal. Most energy production related accidents are from the production of fossil energy resources. An example is the recent coal mine accident in Soma in Turkey where at least 245 workers lost their lives [13]. Coal mining related deaths are also relatively common in China [14]. Fossil fuels have some positive sides also. They provide a high amount of energy, they are available at all times and they can easily be transported. Coal can be used for heating and to produce electricity, and oil is mostly used for transport.

Some examples of renewable energy resources are wind, hydro, wave, solar, and geothermal heat. The renewable resources normally pollute less than the fossil fuels and does not have that much impact on the climate. However, some of the renewable energy resources are not available at all times, such as solar and wind energy. These are only available when the

weather conditions are right. We therefore need to use another energy source when these resources are not available, or store the energy they produce for later use. Also, especially for solar and wind energy there are visual constructions, such as solar photo voltaic plates and windmills, which some people does not like the view of. With hydro power they build huge dams to contain the water, which leads to landscape changes. There is also a slight possibility that the dam will break. The energy production from renewable resources is increasing for each year, but their contribution to the total energy consumption is still low compared to the contribution of fossil fuels. The renewable energy amount produced is often lower than those of the nonrenewable energy sources. Also, the installations often have high start up costs, so it might not be economical to produce renewable energy with the current prices of fossil fuels. It is best to use the renewable energy locally with consideration of which of the renewable energy sources are most economical to produce. If there is much sun and little wind it makes more sense to focus on solar power than windmills.

1.2 Geothermal energy

In this thesis we will look further into geothermal energy, which is heat collected from under the earths surface. This geothermal energy has a great potential to help supplying energy to cover the increasing demand for energy in the world.

The benefits of geothermal energy is that it is available at all times, and not dependent on the weather. This gives us a continuous source of heat and energy so we do not need a backup source. It can also act as a backup source for other renewable energy sources that are not available at all times. The deeper we drill towards the center of the earth, the hotter it will be. This makes geothermal energy available all over the world. There are also some areas that has higher temperatures than average at the same depth, which are called geothermal hot spots. These areas are often along the tectonic plate borders.

Heat moves from warm areas to cold areas, so the heat we collect will be replenished, and if we collect heat at the same rate it is replenished, then we will have an unlimited resource. If we however collect the heat from the reservoir faster than it is replenished, then we must wait for enough heat to return from the surrounding areas before we can collect more heat from the reservoir.

Production of geothermal energy pollutes little, and it only takes up a small space above ground. It has however high up front investment costs, so we need to use geological data to locate good places to drill, followed by a test drill to confirm that it is suitable for extraction of heat. If the site seems good we can drill injection and production wells. The drilling costs typically scale exponentially with depth, and deeper than 6 km is usually not economical to drill anymore as the drilling costs becomes too large. Because the geothermal wells have a larger diameter than oil and gas wells, this increase the drilling costs and makes

it harder to drill due to hard rocks, high temperatures and high pressures. Luckily the operation and maintenance costs are low once everything is in place. A geothermal system can lead to increased seismic activity in the area, and land subsidence due to changes in the reservoir.

We can divide geothermal systems into shallow and deep systems. Shallow geothermal systems have a depth from a couple of meters up to a couple of hundred meters, and we typically use the heat to heat up buildings by using heat pumps and heat exchangers. The shallow reservoirs can also be used for cooling in the summer when the temperature in the ground is lower than the surface temperature. These systems are nice for home heating but the temperature is too low to generate electricity. These systems need electricity to run the heat pump. Deep geothermal systems ranges from a couple of hundred meters depth to a couple of kilometers depth. Here we often have a higher temperature, so the geothermal heat can be used for heating, and it can also be used to generate electricity.

Geothermal reservoirs are underground porous hot rocks where water can flow through the reservoir. To collect this heat, cold water is injected in the injection wells. The cold water flows through the reservoirs pores and fractures while absorbing heat from the surrounding hot rock. Heat will be transported with the water as convection, but it will also be transported by conduction. To collect more heat from the surrounding rock, it is good with a high contact surface over a large area, rather than the water flowing fast through a large fracture from the injection well to the production well. The water or steam that reach the production wells will be hotter than the water injected into the injection well. This is illustrated in Figure 1.2.

To generate electricity we typically use a Rankine cycle where we use high pressured water that is heated into steam. This steam will expand through the turbine, generating power. We then condense the steam back into liquid which can be reheated to run the turbine again. We have different kinds of power plants to convert water into steam. Dry steam power plants use the hot steam directly that is pumped up from the reservoir to run the turbine after removing particulate matter that may damage the turbine. Flash steam power plants use high pressured hot water that is converted to flashed steam when introduced to a lower pressure. Binary cycle power plants use the hot water to heat up a secondary fluid with a lower boiling point so it turns into steam that runs the turbine. The turbine is connected to a generator that produces electricity. When the water is cooled it is pumped back into the reservoir to collect more heat.

Always when we transform heat into electricity there will be energy lost. The highest efficiency theoretically possible is the Carnot efficiency, given by

$$\eta_{cycle} = \frac{W_{net}}{Q_H}, \tag{1.1}$$

where η_{cycle} is the cycle efficiency, W_{net} is the net useful work obtained from the system, and Q_H is the amount of heat transferred from the geothermal fluid. The actual efficiency

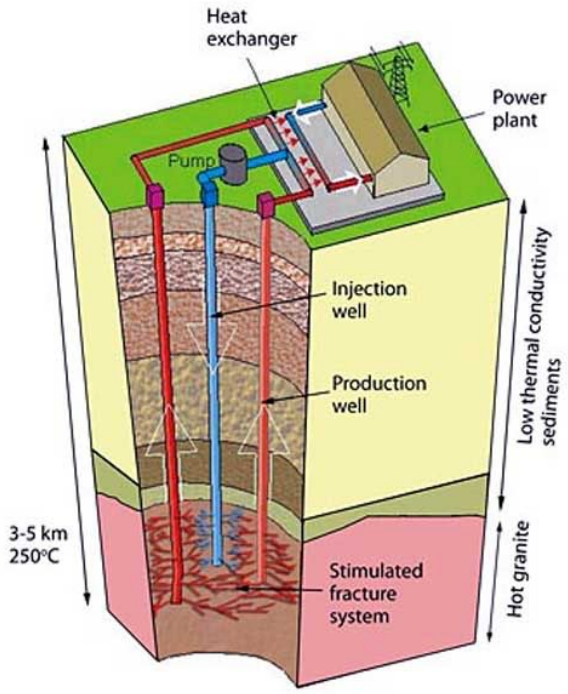

Figure 1.2: A geothermal system where cold water is pumped into the reservoir, and warm water pumped out of the reservoir to run a turbine that generates electricity. *Photo from geothermal-resources.com.au (May 2014)*

will be lower due to friction and other causes.

We will have a continuous heat flow from the center of earth towards the earths surface due to the temperature difference between them. This heat inside the earth is caused by residual heat from the earths creation, and by radioactive decay in the crust. This continuous heat flow will replenish the geothermal reservoir for its lost heat. The average heat flow is $5.9 \cdot 10^{-2}\ W/m^2$ [5].

The geothermal gradient ∇T gives us as relation between the temperature difference ∂T and the difference in depth ∂z. We have that $\nabla T = \partial T / \partial z$. The geothermal gradient will vary at different places on earth, and at different depths due to the inhomogeneities in the temperature differences in the earths crust due to permeability, heat capacity and conductivity differences of the rocks. However, this geothermal gradient is typically 25 degrees Celsius per km depth away from tectonic plate boundaries, and higher near the plate boundaries.

If there is hot water, pores and fractures already in the reservoir it is called a hydrothermal reservoirs, and these reservoirs we can use straight away after drilling the wells. If the reservoir lacks the water, pores and fractures, but got a high temperature and temperature gradient, we can add the missing components to the reservoir and make it an enhanced

geothermal reservoir. Pores and fractures can be created or expanded by pumping high pressure cold water into the reservoir, or by using chemical compounds.

1.3 Mathematical models

To get a better understanding of what happens in the reservoir and how the heat transports between the wells, we create mathematical models that simulates the reservoir. This is important to do before drilling the wells, as the drilling is quite expensive. By making different simulations, we will get an idea of where to add the wells, and which injection rates that could give a high energy production over time.

When we do reservoir simulations, the reservoir is divided into small grid cells where all the geological data and properties such as porosity, permeability and thermal conductivity are defined. A fine scale porosity field is shown in Figure 1.3. Here we see that the porosity varies in the reservoir. The same counts for the permeability. We need our models to account for these variations in porosity, permeability and thermal conductivity, and to simulate the convection and diffusion of the heat transport accurately.

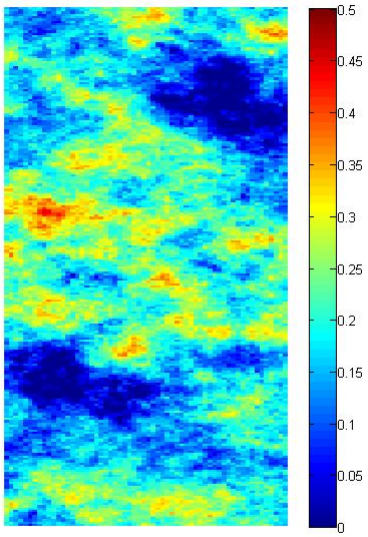

Figure 1.3: Porosity field of a 60x220 grid with porosity ranging from 1e-4 to 0.4423.

The reservoirs are usually quite large though with up to several million grid cells, which is much larger than in our figures with 13200 grid cells. It would be impossible to simulate the large reservoirs on the fine scale due to the large amount of grid cells we have to calculate equations on. The calculations and simulations takes a lot of computational

power and time. This makes it necessary to reduce the amount of grid cells so we can do the simulations on a reasonable time scale. This however makes the simulation less accurate, so we have to comprise between accuracy and computational time. The goal is to have high accuracy and low computational time in these simulations.

In this thesis we will look into ways to combine small grid cells into larger coarser grid blocks by using a coarsening algorithm that coarsens the grid based on different indicators. The indicators we use are the logarithmic permeability, velocity and time of flight. We will also use a coarse Cartesian grid. We will implement an upscaling of the properties and equations so they can be solved on the coarse grids, so we can run simulations on the reservoir.

A simulation of the heat transport on a 60x220 celled reservoir and its coarse upscaled 162 celled version is shown in Figure 1.4.

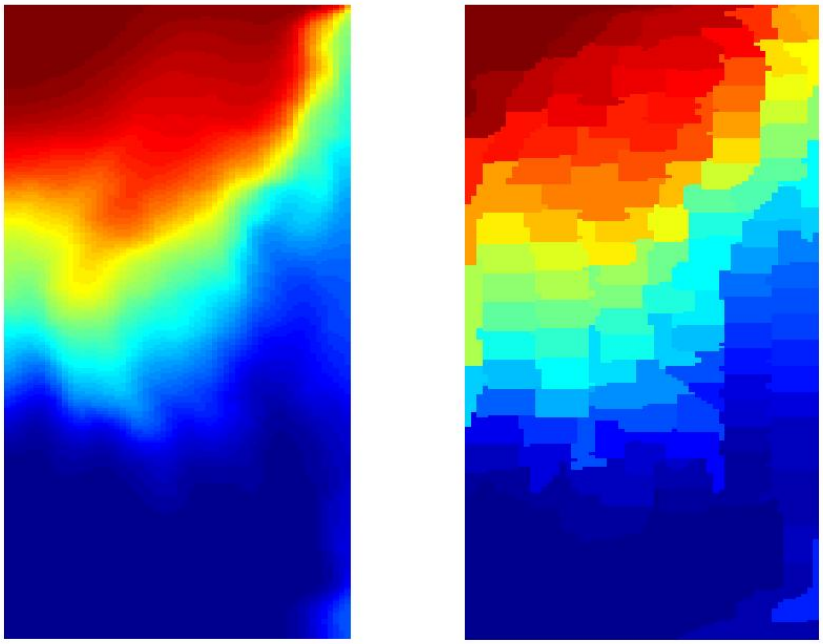

Figure 1.4: A simulation of the temperature in a reservoir with 60x220 cells on the left. On the right the simulation done on a coarse scale version with 162 cells. Injection of cold water is in the lower left corner, and the production is done in the upper right corner.

As we see in Figure 1.4, the accuracy is less for the coarsened grid than the fine grid, but the main aspects and temperature flow lines are still preserved.

We will take inspiration from SINTEF's work on upscaling the transport equation. They were however motivated by oil transport in oil reservoirs. We will look at heat transport

simulations in geothermal reservoirs, so we must add an additional diffusive term compared to the transport equations used for oil reservoirs where diffusion is not important. The convective part of the transport equation is also important in geothermal heat transport. Therefore we must implement models that can handle the whole spectrum from convection dominated to diffusion dominated transport. Because we already have the upscaled convection dominated transport equation from SINTEF, what we will do is to expand this model to also work for diffusion dominated heat transport. We will first calculate the pressure equation on fine scale to get the fluxes, and then upscale and solve the transport equation in regards to temperature on the coarse grid. We will first explore the behavior of this upscaling on a simple homogeneous grid where the porosity, permeability and thermal conductivity are the same in the whole reservoir. After the simple reservoir, we will look into heterogeneous grids done on a formation called SPE10 to see how our model is behaving for convection dominated and diffusion dominated heat transport in a heterogeneous medium. We hope our heat transport upscaling model will be of help to questions like for where to drill the wells, how many wells we should have, which injection and production rates are good, and how much energy we will produce from the geothermal reservoir.

Chapter 2

Flow in porous media - properties and equations

In this chapter we will introduce various rock and fluid properties and equations that are used for modeling fluid and heat flow in porous media. This chapter is based mainly on the sources [6], [9], and [8], and also [7] for the heat transport and energy equation. All our models will be on one phase flow, and we will only use two dimensions for simplicity, because we will consider horizontal flow.

2.1 Fluid properties

Fluid properties such as density and viscosity are determining how the fluid will flow, and along with heat capacity it has effect on the heat transport of the fluid. A fluids properties will usually vary with temperature and pressure. These properties we need for Darcy's law, the pressure equation and the energy equation that we will define later in this chapter.

The density of a substance is defined as its mass divided by its volume.

$$\rho = \frac{m}{V} \tag{2.1}$$

Here ρ is the density, m is the mass, and V is the volume. The density of water is approximately 1000 kg/m^3.

The viscosity, μ, measures a fluids resistance to flow due to internal friction. Fluids with a higher viscosity, such as syrup, will not flow as easily as fluids with lower viscosity, such as water.

To raise the temperature of different matters by the same amount of degrees, you have to provide different amounts of heat depending on the heat capacity, C, of the matter.

The heat capacity will vary by the volume of the system, and also by its temperature and pressure. The specific heat capacity, c, we get when we divide the heat capacity by the mass of the system.

$$\text{Specific heat capacity, } c = \frac{\text{Change in heat energy}}{\text{Change in temperature} \cdot \text{mass}} = \frac{\Delta Q}{\Delta T m}. \tag{2.2}$$

We keep either the volume or the pressure constant when measuring the heat capacities, and we denote these heat capacities c_V or c_p, depending on which of the variables we keep constant. These equations are given by

$$c_V = \left(\frac{\partial e}{\partial T}\right)_V \tag{2.3}$$

and

$$c_p = \left(\frac{\partial h}{\partial T}\right)_p, \tag{2.4}$$

where e is the specific internal energy, T is the temperature, and V and p denotes that we keep the volume or pressure constant. h is the specific enthalpy given by $h = e + p/\rho$.

2.2 Porosity

A porous medium consists of solid and void spaces, where the voids are called pores and the solids are called matrix. If these pores are interconnected, fluid can flow through them. Examples of porous media are sand, rocks, and sponges.

Because a microscopical point of a porous medium will be either in the matrix or in the pores, we will use an average called representative elementary volume (REV). This is the smallest volume where we can get representative measurements of averaged values. This volume should be larger than the pore scale, but smaller than the total domain volume.

The porosity is defined as the pore volume fraction of the total volume of a REV. However, there can be pores that are isolated from other pores as seen in Figure 2.1, and are therefore not in the pore network, or pores that have dead ends.

We will use the effective porosity which include only the interconnected pores, and not those who are isolated or leads to nowhere. The porosity ϕ is given by:

$$\phi = \frac{\text{interconnected pore volume}}{\text{total volume of REV}} = \frac{V_{pore}}{V_{tot}}. \tag{2.5}$$

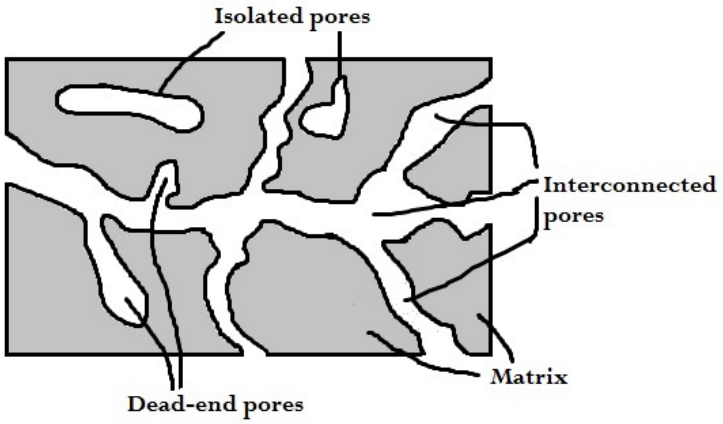

Figure 2.1: A porous media with isolated, dead end and interconnected pores. The shaded part is the matrix.

If a property, like porosity, is the same in the whole domain, the porous medium is called homogeneous. If the property is varying with position, the medium is called heterogeneous.

2.3 Darcy's law

Darcy's law is named after Henry Darcy, who in 1856 published a study on sand filter design [6]. His experiment, as illustrated in Figure 2.2, was done by filling a column with sand, then letting water flow through the column with volumetric flow rate $\mathbf{v}_{Darcy}$. The cross sectional area of the column we denote A. On two spots in the column with a length L between them there are two tubes that penetrate the column with their entrance at a height z_1 and z_2 above a set datum. The hydraulic heads, h_1 and h_2, tells us how high the water rise in the two tubes above the datum.

After numerous experiments, he found the relation

$$\mathbf{v}_{Darcy} = \kappa \frac{A\,(h_2 - h_1)}{L}. \tag{2.6}$$

Here, κ is a proportionality coefficient, and it is also referred to as the hydraulic conductivity.

If we rewrite this, defining the volumetric flow flux $\mathbf{v} = \frac{\mathbf{v}_{Darcy}}{A}$ and the hydraulic head $h = \frac{p}{\rho g} + z$ and the proportionality coefficient $\kappa = \mathbf{K}\frac{\rho \mathbf{g}}{\mu}$, we get the modern Darcy's

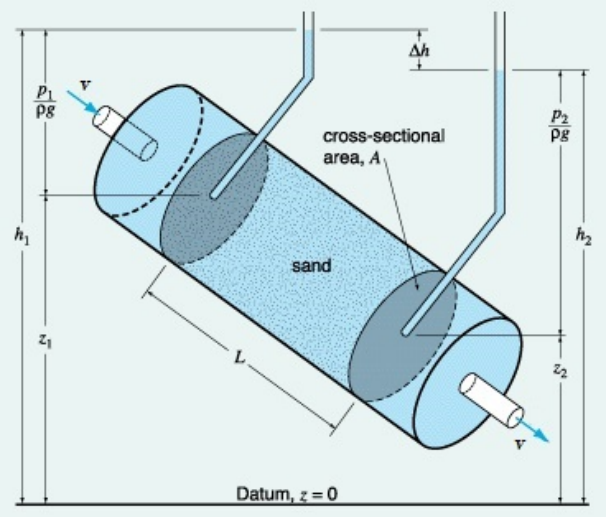

Figure 2.2: An illustration of Darcy's experiment that lead to Darcy's law.
Figure: hercules.gcsu.edu (May, 2014)

law:

$$\mathbf{v} = -\frac{\mathbf{K}}{\mu}\left(\nabla p - \rho \mathbf{g}\right). \tag{2.7}$$

Here, $\mathbf{v}$ is the volumetric velocity flux, $\mathbf{K}$ is the permeability tensor of the rock, μ is the viscosity of the fluid, p is the pressure, ρ is the density of the liquid, $\mathbf{g}$ is the gravitational vector.

The permeability, $\mathbf{K}$, gives us an indication of how easily fluids flows through the porous medium. The higher the permeability is, the more easy the fluid will flow. If the permeability is constant in the reservoir, the medium is homogeneous, while if the permeability changes with position, the medium is heterogeneous.

If a property have different values in different directions, the medium is called anisotropic, while if the values are the same in all directions it is isotropic. An example is if a fluid would flow better horizontal rather than vertical due to different permeabilities in the different directions.

2.4 Conservation of mass

The law of conservation of mass states that mass cannot be created or destroyed within a closed system.

This means that if we consider an arbitrary volume, Ω, the mass change in Ω will equal the mass flow over the boundary, S, plus the source inside the volume. In mathematical

terms, this is written as:

$$\int_\Omega \frac{\partial}{\partial t}(\phi\rho)\,\mathrm{d}\Omega = -\int_S \rho\mathbf{v}\cdot\mathbf{n}\,\mathrm{d}S + \int_\Omega Q\,\mathrm{d}\Omega. \tag{2.8}$$

Here, ϕ is the porosity, ρ is the density, $\mathbf{v}$ is the velocity, $\mathbf{n}$ is the outward unit normal vector, and Q is the net mass production in Ω from the sources and sinks. We use the divergence theorem to convert the boundary integral to a volume integral, so we get

$$\int_\Omega \left(\frac{\partial}{\partial t}(\phi\rho) + \nabla\cdot(\rho\mathbf{v}) - Q\right)\mathrm{d}\Omega = 0. \tag{2.9}$$

Because this equation is valid for any arbitrary volume we can remove the integral, and we are left with

$$\frac{\partial}{\partial t}(\phi\rho) + \nabla\cdot(\rho\mathbf{v}) - Q = 0. \tag{2.10}$$

If we assume that the porosity and density are constant, and does not change in time, we can simplify this to

$$\nabla\cdot(\rho\mathbf{v}) = Q. \tag{2.11}$$

By adding the velocity from Darcy's equation, (2.7), and assuming that our fluid is incompressible, we get the pressure equation

$$-\nabla\cdot\left(\frac{\mathbf{K}}{\mu}(\nabla p - \rho\mathbf{g})\right) = \frac{Q}{\rho}, \tag{2.12}$$

which equals to zero if we have no net source or sinks.

We will neglect gravity because the flow will be mostly horizontal, and we will work with a 2D-grid. We then get the simpler pressure equation

$$-\nabla\cdot\left(\frac{\mathbf{K}}{\mu}\nabla p\right) = \frac{Q}{\rho}. \tag{2.13}$$

2.5 Heat transport

Heat can be transported by three different ways, by conduction, convection, and radiation. We will neglect the radiative effects in this thesis because it has minimal influence on the heat transfer.

We have conduction when energy is transfered from energetic particles to less energetic particles. When the molecules vibrate or collide they will transfer energy to each other. This means that the molecules will have to be in very close range of each other to transfer the energy. When we have a transfer of heat from hot to cold areas due to random motion it is called conduction or diffusion. The conduction is described by Fourier's law, which is written mathematically as

$$\mathbf{q}_{cond} = -\mathbf{k}\nabla T. \tag{2.14}$$

Here, $\mathbf{q}_{cond}$ is the conductive heat flux, $\mathbf{k}$ is the thermal conductivity of the material, and T is the temperature, which makes ∇T the temperature gradient. The thermal conductivity, $\mathbf{k}$ varies with temperature and can be a tensor if the material is anisotropic, and it can vary with location if the material is nonuniform. The heat will move from parts with higher temperature to parts with lower temperature.

Convection is when we have movement of fluid, and is what we see when water is boiling. Convection is the combination of advection, which is the bulk movement of the fluid, and conduction or diffusion, which is the individual random movement. Convection can only happen in gases and fluids because solids cannot move. The convection can either be natural, caused by buoyancy changes due to changes in the density from temperature differences, or it can be forced by an external force, for instance a fan, pump or mixer. We will assume that we have a local thermal equilibrium so that the temperature of the rock and fluid is equal.

The convective heat flux is given by

$$\mathbf{q}_{conv} = \rho c_p \mathbf{v} T, \tag{2.15}$$

where ρ is the density, c_p is the specific heat capacity measured with constant pressure, v is the velocity, and T is the temperature.

2.6 Conservation of energy

Similar to the law of conservation of mass, we have that the law of conservation of energy states that energy cannot be created nor destroyed, it can only change forms. So in an isolated system, the total energy will always stay the same.

Energy can be divided into different types. Some examples are kinetic energy, potential energy, electromagnetic energy, chemical energy, and thermal energy. The flow in our porous medium is however quite slow, so we can neglect the kinetic energy. We also neglect the other types of energy and the gravitational effect, and focus only on thermal energy.

We assume a local thermal equilibrium, so that the temperature difference between the solid and the fluid in the REV is much smaller than the temperature difference in the whole reservoir. We also assume there are no phase changes, and no work done by or on the system.

Then the thermal energy in an arbitrary volume, Ω, is conserved, and the change in thermal energy in Ω is equal to the net sum of thermal energy flowing into the volume plus the change in energy caused by conduction, plus heat sources. We also assume the heat capacity and the density varies slowly with time.

We set the temperature of the rock and fluid equal, $T_s = T_f = T$, and get the energy equation

$$(\rho c)_{eff} \frac{\partial T}{\partial t} + (\rho c)_f \mathbf{v} \cdot \nabla T - \nabla \cdot (\mathbf{k}_{eff} \nabla T) = Q_{eff}. \tag{2.16}$$

The first term in the energy equation (2.16) is called the transient term, the 2nd term is the convection term, the 3rd term is the diffusion term, and the 4th term is the source term.

In the energy equation, (2.16), we have the effective heat capacity per unit volume

$$(\rho c)_{eff} = (1 - \phi) (\rho c_s)_s + \phi (\rho c_p)_f , \tag{2.17}$$

the effective thermal conductivity

$$\mathbf{k}_{eff} = (1 - \phi) \mathbf{k}_s + \phi \mathbf{k}_f, \tag{2.18}$$

and the effective heat production per unit volume of the porous medium

$$Q_{eff} = (1 - \phi) Q_s + \phi Q_f. \tag{2.19}$$

In these equations, ϕ is the porosity, ρ is the density, T is the temperature, $\mathbf{v}$ is the velocity, Q is the heat production per unit volume, $\mathbf{k}$ is the thermal conductivity, c_s is the specific heat capacity of the solid, and c_p is the specific heat capacity of the fluid with the pressure held constant. The subscripts s and f refers to solid and fluid respectively.

2.7 Péclet number

We wish to have a dimensionless number that tells us if the convection or diffusion is dominating the heat transport, and for this we will use the Péclet number. The Péclet

number, Pe, is defined as

$$Pe = \frac{L\mathbf{v}\rho c_p}{\mathbf{k}}. \tag{2.20}$$

Here, L, is the characteristic length, $\mathbf{v}$ is the velocity, ρ is the density, c_p is the specific heat capacity, and $\mathbf{k}$ is the thermal conductivity. If the Péclet number is high, the convection dominates, while if the Péclet number is low, the diffusion is dominating the heat transport in the reservoir.

Chapter 3

Numerical methods

The mathematical equations we deal with to describe our system are the partial differential equations presented in Chapter 2. We can only solve them analytically for a few simple cases. We can however get good approximate solutions by using numerical methods. With numerical methods, we discretize our reservoir into a grid with many grid cells, that each contain information about the properties in that grid cell. The time it takes to solve these equations depends on how many cells we solve the equations for, which accuracy we want, and if our solver is efficient.

In this thesis we will use a method called the finite volume method. The finite volume method is a much used discretization method for various types of partial differential equations like elliptic, hyperbolic and parabolic equations. Some of the advantages of this method is its robustness, that it can be used on various geometries and on unstructured grids, and it is also locally conservative in regard to fluxes [1].

In this method, the domain is divided into control volumes, where we turn the volume integrals of the equations we wish to solve into surface integrals, by using the divergence theorem. We then evaluate the fluxes over the boundary of each control volume.

We have different sub-methods of the finite volume method. In this thesis we will use the two-point flux approximation method and the upwind method to discretize the pressure equation (2.13) and the energy equation (2.16), that we recall as

$$(\rho c)_{eff} \frac{\partial T}{\partial t} + (\rho c)_f \mathbf{v} \cdot \nabla T - \nabla \cdot (\mathbf{k}_{eff} \nabla T) = Q_{eff}. \tag{2.16}$$

Our boundary conditions will be no flow and no heat transport.

We first solve the discretized pressure equation on fine scale. We only do that once as the flow field will remain constant in time in our chosen model. We use the two point flux approximation method to solve this equation. We then solve the discretized energy equation (2.16) in regards to temperature by first calculating the half transmissibilities, α,

followed by computing the rest of the temperature by using the two point flux approximation method. When we have the fluxes, pressures and temperatures, we solve the whole equation, using the time discretization and the upwind method. These methods we will describe further in this chapter.

The sources used in this chapter are mainly [1], [2], [8] and [9].

3.1 Two-point flux approximation

The two-point flux approximation method is popular due to its simplicity and computational speed. The downside is it is only exact for K-orthogonal grids. For a grid to be K-orthogonal, $\mathbf{n} \cdot \mathbf{k} \parallel \mathbf{d}$ must be satisfied. Here $\mathbf{n}$ is the unit vector normal to the edge between the cells, $\mathbf{k}$ is the thermal conductivity tensor, and $\mathbf{d}$ is the vector from the edge between the cells, to the center of the cell.

Lets consider the diffusive term from the energy equation:

$$-\nabla \cdot (\mathbf{k} \nabla T) = Q. \tag{3.1}$$

In this equation, $\mathbf{k}$ is the thermal conductivity tensor, T is the temperature, and Q is a source term.

It is the same procedure for the pressure equation, (2.13), which we have simplified to

$$-\nabla \cdot (\mathbf{K} \nabla p) = Q, \tag{2.13}$$

where $\mathbf{K}$ is the permeability tensor, p is the pressure and Q is the source term.

We integrate over each grid cell volume.

$$\int_{\Omega_i} -\nabla \cdot (\mathbf{k} \nabla T) \, \mathrm{d}\Omega = \int_{\Omega_i} Q \mathrm{d}\Omega. \tag{3.2}$$

Then we use the divergence theorem.

$$\int_{S_i} (-\mathbf{k} \nabla T) \cdot \mathbf{n} \mathrm{d}S = \int_{\Omega_i} Q \mathrm{d}\Omega. \tag{3.3}$$

Here, $\Omega_i \subset \Omega$, where Ω is the total domain, Ω_i is the volume of each grid cell, and S_i is the boundary of the grid cell i.

If we look at figure 3.1, we have the two grid cells Ω_i and Ω_{i+1}. The black dots represents the cell centers x_i and x_{i+1}, while the red dot is the point $x_{1+1/2}$. The area between the grid blocks is denoted S, and is represented by the orange line. $\mathbf{n}$ is the outward unit

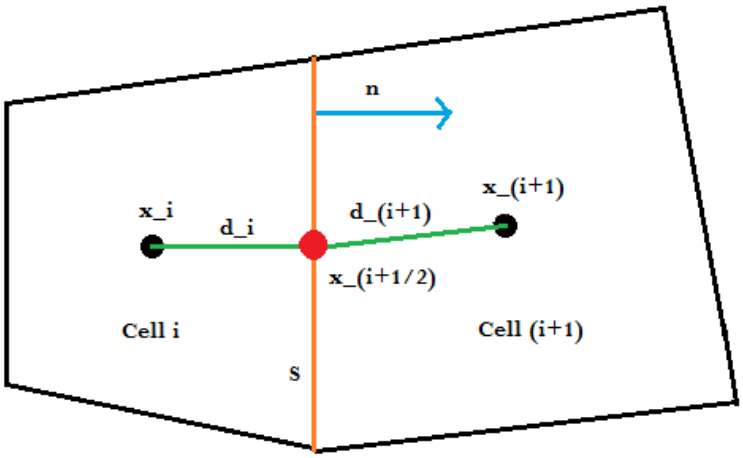

Figure 3.1: Grid cells.

normal vector, which is colored blue on the figure. The green lines are the vectors between x_i and $x_{i+1/2}$, and between $x_{i+1/2}$ and x_{i+1}, and if the grid is K-orthogonal, this will be the same as $\mathbf{k_i n}$ for block i.

We define the half transmissibility α_i as

$$\alpha_i = \frac{S\mathbf{n} \cdot \mathbf{k_i}}{\mathbf{d_i} \cdot \mathbf{d_i}} \cdot \mathbf{d_i}. \tag{3.4}$$

Here $\mathbf{d}_i$ is the distance vector from the centroid of a cell, to the face center of that cell, and S is the area of the face.

The flux q over S in the direction of $\mathbf{n}$ from cell 1 to cell 2 is approximated by

$$q_1 = -\int_S (\mathbf{k}_1 \nabla T) \cdot \mathbf{n} \mathrm{d}S \approx -\alpha_1 \left(T_{face} - T_1\right). \tag{3.5}$$

In the opposite direction, the flux from cell 2 to cell 1 will be

$$q_2 = \int_S (\mathbf{k}_2 \nabla T) \cdot \mathbf{n} \mathrm{d}S \approx -\alpha_2 \left(T_2 - T_{face}\right). \tag{3.6}$$

We want to eliminate T_{face}, so we combine the expressions and get the flux

$$q_{12} = -t_{12} \left(T_2 - T1\right), \tag{3.7}$$

where t_{12} is the transmissibility, given by the harmonic average of the half transmissibilities

$$t_{12} = \frac{\alpha_1 \alpha_1}{\alpha_1 + \alpha_1}. \tag{3.8}$$

We can now find the flux over each edge of a cell, and if we sum the fluxes out of the block minus the fluxes into the block, this should equal the source times the volume of the cell.

$$q_{out} - q_{in} = Q \cdot \Omega. \tag{3.9}$$

We then do this for each cell in the grid, which gives us a complete set of linear equations for solving T_i.

3.2 Upwind method

The upwind method considers the direction of the flow, and the positive direction of the flux over a boundary will be the upwind side, while the negative direction will be the downwind side. We use this method on the convective flux term, which is a hyperbolic differential equation on the form

$$\frac{\partial T}{\partial t} + \nabla \cdot (T\mathbf{v}) = 0. \tag{3.10}$$

If we look at the convective term and use the divergence theorem we get

$$\int_{\Omega_i} \nabla \cdot (T\mathbf{v}) \, \mathrm{d}\Omega = \int_{S_i} \mathbf{n} \cdot (T\mathbf{v}) \, \mathrm{dS}. \tag{3.11}$$

We look at the convective flux over the edge S between two cells in the direction of $\mathbf{n}$, then the flux q is determined by the direction of $\mathbf{v}$ by taking

$$r = \int_S \mathbf{v} \cdot \mathbf{n} \mathrm{dS}. \tag{3.12}$$

Then we get the flux for each edge:

$$q = \begin{cases} rT_i & \text{if } \mathbf{v} \geq 0 \\ -rT_{i+1} & \text{if } \mathbf{v} < 0 \end{cases}$$

.

3.3 Time discretization

For the discretization of time for the first term of equation (2.16), we use the backward Euler method. This method is implicit, which makes it stable, but with the cost of longer computational time than explicit methods.

To show the time discretization, we simplify the energy equation (2.16) into the following system of ODEs

$$\frac{\mathrm{d}T}{\mathrm{d}t} = G\left(T, t, \mathbf{v}\right). \tag{3.13}$$

Here, T is the temperature, and G is the operator containing the discretization of the convective and conductive part of equation (2.16) and the source term. G will depends on the fine scale temperature,T, on time, t, and on the mass fluxes $\mathbf{v}$ from Darcy's law (2.7).

Using the backward Euler method, the discretized equation is given as

$$T_{k+1} = T_k + G\left(T_{k+1}, t_{k+1}, \mathbf{v}_{k+1}\right)\Delta t, \tag{3.14}$$

where Δt is the time step size.

Since this is an implicit, non-linear equation, with T_{k+1} occurring on both sides, we have to use some other method to solve this system for each time step, for instance the iterative Newton-Raphson method.

In our program we compute the Jacobian matrix and the residuals before using the Newton-Raphson iteration to help solve the equations.

Chapter 4

Coarse Scale Discretization

The grids we use on geothermal reservoirs are often very large with possibly several million small grid cells to include fine scale variations that exist in our reservoirs. This gives a good resolution, but it also makes the computational time way too long for our modern computers, because of the large system of equations (that we discussed in Chapter 3) that we must solve for each discretized cell in our reservoir. We therefore want to have a smaller amount of grid cells to solve these equations on to make the computation faster. To get a smaller amount of grid cells we combine several fine scale grid cells into larger coarse scale grid blocks. By coarsening the grid we lose resolution and accuracy. The goal of this coarsening is to do it in a way that preserve the main features of the heat transport while reducing the amount of grid cells.

To solve the energy equation, we will first solve the pressure equation on fine scale to get the fluxes in the reservoir. We then solve the energy equation on the coarse grid using the fine scale fluxes. We must upscale the fine scale properties that is used in the energy equation such as porosity, heat capacity and thermal conductivity to be able to solve the equation on coarse scale.

The upscaled porosity we find by taking the pore volume of the coarse grid block and divide it on the total coarse grid block volume.

The heat capacity is a constant that depends on the material, and not on the size of the grid blocks, so if the material has different heat capacities we would have to average it to get an effective heat capacity, but in this thesis we will assume it is the same in the whole reservoir.

To get the upscaled thermal conductivity we can average the fine scale values into one coarse scale value, or we can do a flow based upscaling. We have chosen to do flow based upscaling where we use Fourier's law to find the upscaled thermal conductivity. This will be described better later in this chapter.

It is hard to know what is the best method to combine cells when upgridding to minimize

the error. It is also hard to know how to best define the combined properties and how to discretize the energy equation on the upgridded coarse grid. The coarse grid that gives the least error varies from case to case, depending on the structure of the fine scale reservoir. In Chapter 5, we will try a few different grids to see which errors they give for a few different examples. The upgridding and upscaling is mostly based on [10] where [11] and [12] is included, and we also use [9].

4.1 Upgridding

In this thesis we will use different ways to upgrid the fine grid into a coarse grid. We will base the upgridding on parameters such as permeability, velocity, and time of flight, and we will also upgrid with Cartesian grids. This parameter based upgridding is from the work done in [11] and [12].

The simplest way to upgrid is by upgridding with a Cartesian grid. Lets say we have a fine grid that is 25x25 cells, then we can upgrid it to for example a 5x5 grid, or a 9x6 grid, or to what seems most reasonable. These two examples are shown in Figure 4.1.

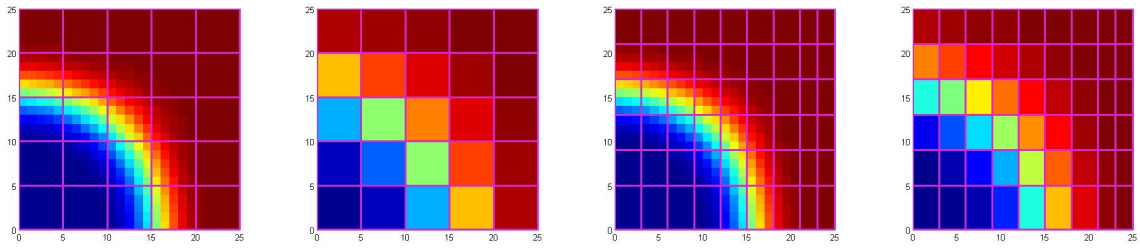

Figure 4.1: Two examples on cartesian upscaling of grids, first a fine scale grid upscaled to a 5x5 grid, then a fine scale grid upscaled to a 9x6 grid. The coarse grid blocks are outlined with pink lines.

Because the coarse grid block edges has to correspond to the fine grid cell edges, some coarse grid blocks will be smaller or larger than the rest if the edges does not correspond. This we can see in Figure 4.1 for the 9x6 coarse grid.

In this thesis we will also use the logarithm of the parameters absolute permeability, velocity at the cell center, and the product of forward and backward time of flight as indicators for how our coarse grid should be made.

The velocity at the cell center is found by transforming the face-based flux field to a constant velocity per cell. The time of flight is found by solving the equation

$$\nabla \cdot (\mathbf{v} T_{oF}) = \phi, \tag{4.1}$$

using the upwind method and multiplying it with the reversed time of flight. Here $\mathbf{v}$ is the Darcy velocity, T_{oF} is the time of flight, and ϕ is the porosity.

For these indicator based coarse grids, we want to separate high flow regions from the regions with low flow, we want to limit the amount of flow through a grid block so there is not too much flow, and we do not want too small grid blocks, so we choose an upper and lower bound respectively. These bounds will affect how many grid blocks we end up with. This type of upgridding is developed in [11] and [12].

In short, these are the steps we use when upgridding, and we will describe them in more detail below:
- Find logarithmic scaled indicator values,
- Divide grid into bins based on indicator values,
- Merge small grid blocks below lower volume bound into larger grid blocks,
- Refine and divide grid blocks with flow above upper flow bound,
- Merge grid blocks that are below lower volume bound.

We will show an example of the upgridding steps based on the velocity indicator for an SPE10 formation where the fine grid is 13200 cells.

To create these coarse grids, we first find the indicator values for each cell, then we do a logarithmic scaling. After that, we divide the cells into ten or another number of uniform bins. After doing this for our example SPE10 grid, we now have 647 cells as we can see in Figure 4.2.

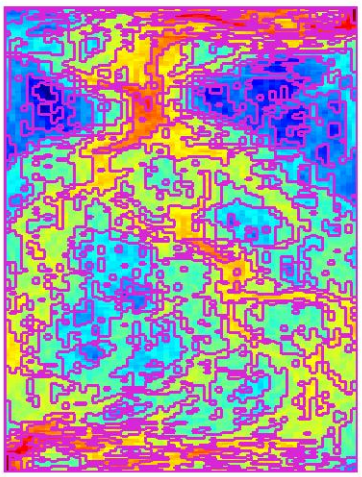

Figure 4.2: Velocity indicator divided into ten bins, which gives us 647 cells. Many of these cells are quite small, while other cells are quite large.

The fine grid has 13200 cells, so this is a nice improvement, but many of the blocks are smaller than our lower volume limit, so we merge the small grid blocks together.

The merging algorithm merges the blocks smaller than the lower volume bound with the neighboring blocks that have the most similar indicator value. The result of this merging we can see in Figure 4.3.

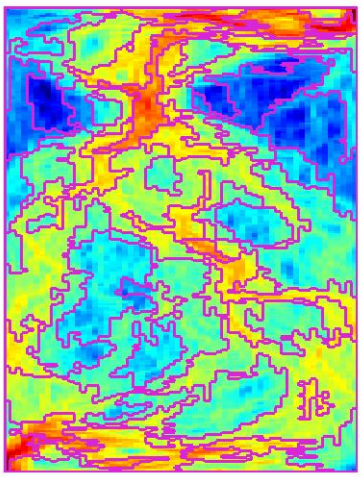

Figure 4.3: Velocity based grid after first merging, we now have 70 cells. Some of these cells are rather large.

The merging might lead to flow above the upper flow bound through some of the blocks, so we must then refine those blocks with a refinement algorithm. This algorithm starts at the cell furthest away from the block center, and letting it add neighboring cells until the upper bound is exceeded, and it is repeated until the indicator values of the remaining cells inside the block is below the threshold. There are a few different refinement algorithms that has a bit different methods of adding cells to the blocks. The different algorithms yields slightly different results. By using one of the methods on the previously merged grid, we now increase our amount of cell blocks to 224 as we can see in Figure 4.4.

After refining the blocks, we might have some blocks that violate the lower volume bound again, so again we merge blocks with the merging algorithm. Usually we finish the merging and refining at this point. There might still be some upper flow bound violations, but a few violations are usually not causing too much problems. It would also be too time consuming to run the refining and merging algorithms until both the bounds are satisfied, which may never happen with the bounds we choose if they keep making blocks that needs refining or merging in the high flow regions. We can see the result from the merging in Figure 4.5.

The result from this merging and refining for the different indicators is shown in figure 4.6. We have here used the refine and merging methods we encountered most commonly, but there are other methods that produce more Cartesian grids or has a different criteria for defining neighboring grid cells. More info on this is found in [11] and [12].

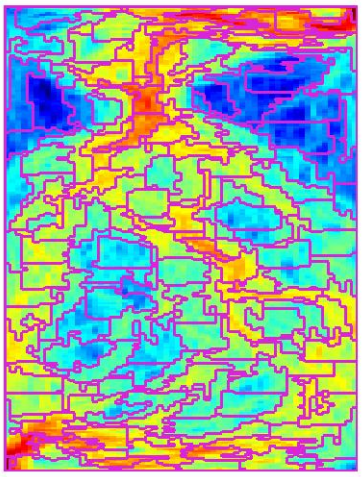

Figure 4.4: Velocity based grid after refining the merged grid blocks with higher flow than the upper limit. This gives us 224 cells.

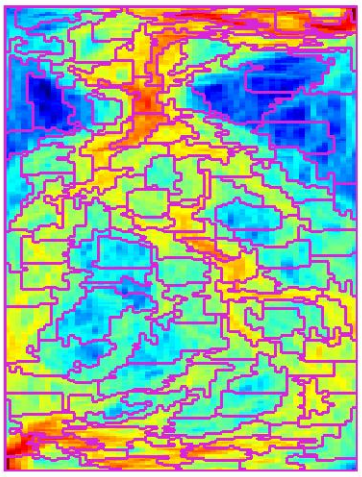

Figure 4.5: Velocity based upgridded after merging, refining and merging. We here have 132 cells.

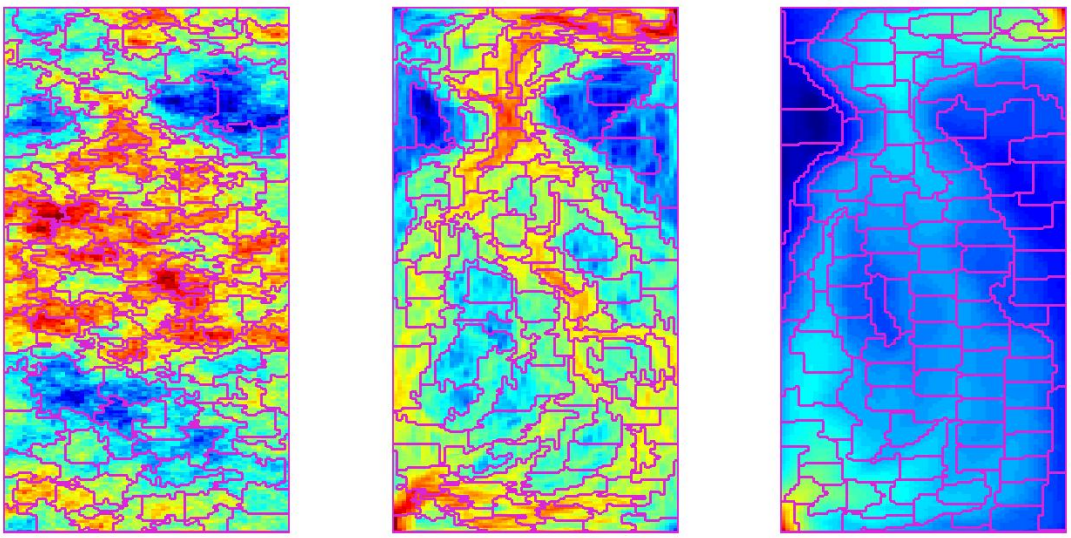

Figure 4.6: The permeability, velocity and time of flight indicators with the resulting coarse grid, with 135, 132 and 119 grid blocks respectively.

4.2 Transport upscaling

By choosing a coarser grid, we have to find a way to solve the energy transport equation (2.16) on the coarse grid.

$$(\rho c)_{eff} \frac{\partial T}{\partial t} + (\rho c)_f \mathbf{v} \cdot \nabla T - \nabla \cdot (\mathbf{k}_{eff} \nabla T) = Q_{eff}. \tag{2.16}$$

Because we combine several fine scale grid cells into coarse scale grid blocks, we have to upscale the parameters, such as porosity and thermal conductivity into one value per cell. It is not so easy to know how to upscale these parameters because they vary in the fine cells within the coarse grid, and different upscaling techniques can range from good to bad depending on the complexity of the fine scale field, and the method used.

The upscaled porosity we find by taking the pore volume of the coarse grid block and divide it on the total coarse grid block volume.

The heat capacity is a constant that depends on the material, and not on the size of the grid blocks, so if the material has different heat capacities we would have to average it to get an effective heat capacity, but in this thesis we will assume it is the same in the whole reservoir.

The source term in the energy equation is upscaled by accumulating the fine scale source

terms within a coarse scale grid block.

A similar equation without the diffusive term has been upscaled before [11], [12], but we will also add the diffusive term to the upscaling of the equation so it will also be valid for the diffusive heat transport, and not only valid for pure heat transport without diffusion.

Upscaling of the convective term

The pressure equation we found in Chapter 2 and discretized in Chapter 3 we solve on the fine scale grid to get the fine scale fluxes. This we only have to do once because we assume a constant flow field. We can sum the fluxes over the edges of the fine grid cells in the coarse grid blocks to get the upscaled convective fluxes for the convective term in the energy equation (2.16).

Upscaling of the conductive term

We need to know the coarse cell centers, face centers and face normals to be able to solve the energy equation when calculating the upscaled conduction term.

To find the coarse cell centroids, we take the average of the fine cell centroids within the coarse grid block. Then we assign the coarse cell centroid to the fine cell centroid closest to the average coarse cell centroid to assure it lays within the coarse cell block. An example of this can be seen in Figure 4.7 for an 8x8 Cartesian grid.

We also do similar for the coarse face centroids, by finding the closest fine cell face centroid to the average of the fine scale face centroids corresponding to the face of the coarse grid block. This is shown in Figure 4.8.

We find the coarse face normals by adding the fine face normals that corresponds to that coarse face.

These methods with averaging and assigning the centroids to the closest fine centroids will give some error when the average does not correspond to the fine cell- or face center. As we see on Figure 4.7, none of the averaged coarse cell centers correspond to a fine cell center. For the average coarse face centers in Figure 4.8 we see that some of them correspond to a fine scale face centers while other does not. However, with this method where we force the coarse cell and face center to correspond to a fine scale cell or face center we assure the coarse cell centers will lay within the coarse cell, and the coarse face centroids will lay on the coarse cell edge. This may not be the case if we only chose the average cell center and face center. The error should be small, and if the average and the chosen centers correspond we have zero error because of this way of choosing centers.

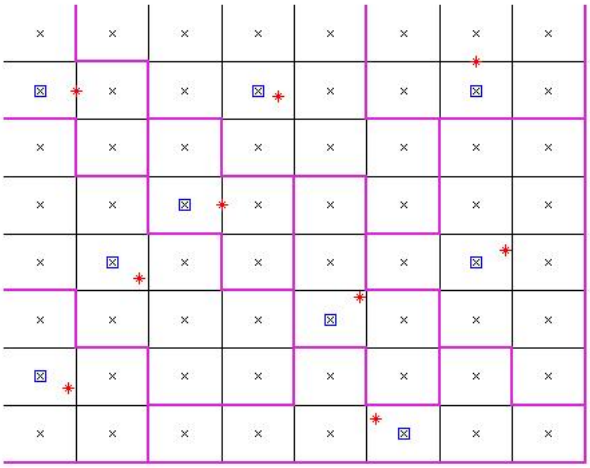

Figure 4.7: New cell centers of the coarse grid blocks. The coarse grid blocks are marked with pink bold lines, the fine scale cell centers are marked with black 'x', the average coarse cell centers are marked with red stars, and the cell centers we will use are the fine scale cell centers closest to the average coarse scale cell centers, which is marked with a a blue square.

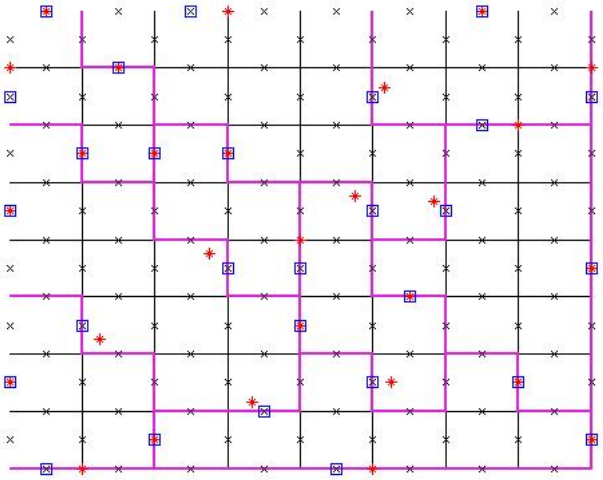

Figure 4.8: New face centers of the coarse grid blocks. The coarse grid blocks are marked with pink bold lines, the fine scale face centers are marked with black 'x', the average coarse face centers are marked with red stars, and the face centers we will use are the fine scale face centers closest to the average coarse scale face centers, which is marked with blue squares.

Thermal conductivity upscaling

For the thermal conductivity in the conductive term in the energy equation (2.16) we will use a flow based upscaling method. This method is often used for upscaling permeability, where it is more robust and accurate than other methods such as averaging [11]. In the flow based upscaling method we use the coarse boundary heat fluxes along with Fourier's law on the coarse grid to find the upscaled thermal conductivity for the coarse cell blocks.

Figure 4.9 is used to illustrate this method. We here have different thermal conductivity values in each of the 8 fine scale grid cells, and we wish to find one effective value for the coarse grid block. We know the pressures, temperatures, areas of the sides, and length between the sides of the coarse grid block edges and the heat fluxes.

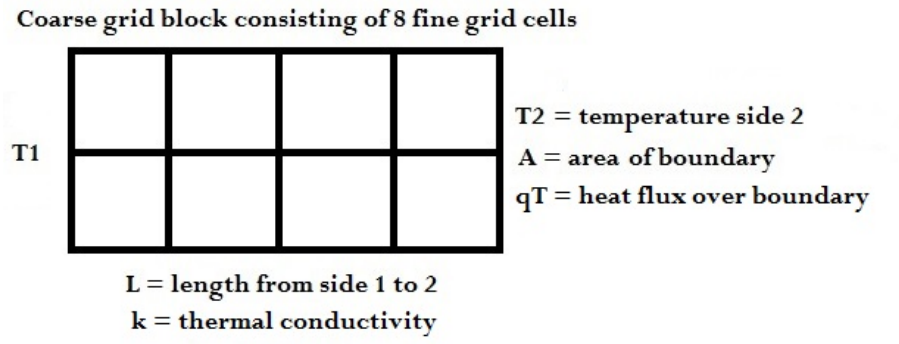

Figure 4.9: A coarse grid block consisting of 8 fine grid cells, where we calculate the upscaled thermal conductivity by solving Fourier's law.

To find the upscaled thermal conductivity tensor $\mathbf{k}_x$, where x is denoting x-direction, we use Fourier's law written as:

$$\mathbf{k}_x = \frac{q_T L}{A\,(T_2 - T_1)}. \tag{4.2}$$

Here, q_T is the heat transfer rate through the boundaries normal to the x-direction, A is the cross-sectional area, L is the length between the boundaries. T_1 and T_2 denote the temperatures on the boundaries normal to the x-direction. We do the same to find the y component of the thermal conductivities for each grid block [9].

After finding all the upscaled parameters, we can calculate the upscaled diffusive term the same way as described in Chapter 3 by using the two point flux approximation.

Now we have upscaled all the terms of the energy equation, and we will solve the equation in regards to temperature like we did in Chapter 3 with the implicit upwind scheme.

Chapter 5

Results

In our results, we wish to see what effect it has to add the diffusive term of the energy equation (2.16) into the MATLAB Reservoir Simulation Toolbox framework. This framework has a solver for the equation without the diffusion term, but we have modified it to solve the energy equation with the diffusive term. In all the plots the injection well is in the lower left corner, while the production well is in the upper right corner.

5.1 MATLAB and MATLAB Reservoir Simulation Toolbox

For the results we use the programming language MATLAB (Matrix Laboratory) developed by MathWorks. This program is great for numerical computation, visualization and it is simple to program in.

We use the MATLAB Reservoir Simulation Toolbox (MRST), developed by SINTEF [4] for our reservoir simulations. This toolbox has useful methods and solvers for porous media simulations for both single and two-phase flows, and the pressure and transport equation we use we find in this toolbox. We also find the merging and refining algorithms from [11] and [12]. There are also visualization tools that we use, and upscaling methods, and more. This makes MRST a very useful framework for reservoir simulations.

At first, we used and edited some of the examples of the modules already in MRST to familiarize ourselves with how it works. This included doing simulations in time on some of the SPE10 grids. The examples found in MRST are mostly on two phase flows (oil and water), and the diffusive term is not included. After being used to the toolbox, we looked into geothermal reservoirs, where we had to add diffusion into the energy equation solver.

In MRST, there are several similar programs to refine and merge the cells blocks in our

coarse grid. Their difference is in the way they merge and refine the grids, where some methods are more computationally expensive than others. From some tests we found out that the different refinement methods mostly gave similar results, regardless of which method we used. In some cases, some refinement methods were better or worse than others, but most of the time they gave similar results, as is expected. We did a test for the different refinement methods for a time of flight indicator based homogeneous grid. The plots we can see in Figure 5.1, and the results for the temperature in the production well and for the accumulated errors we can see in Figure 5.2.

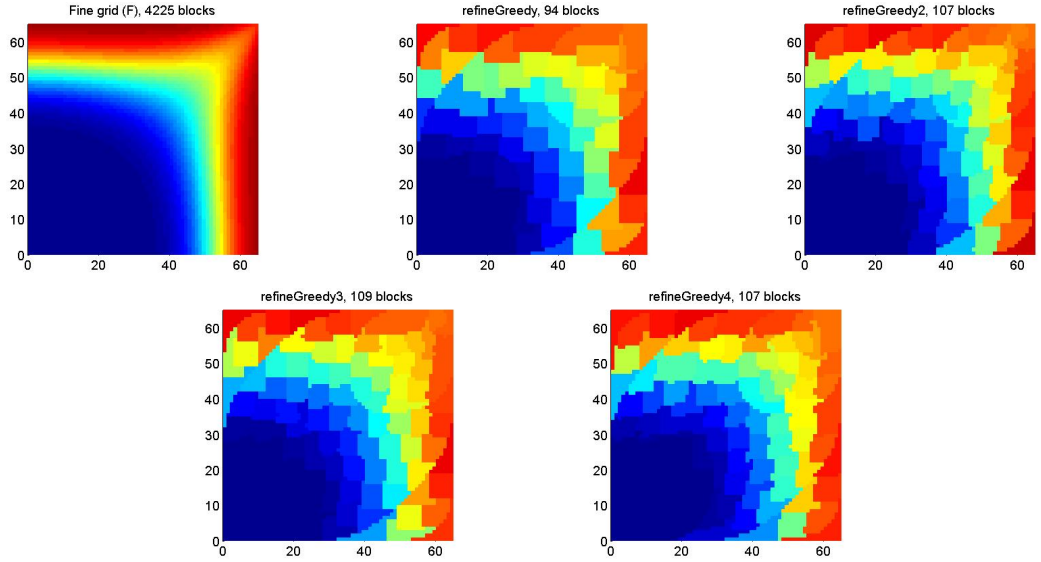

Figure 5.1: The different refine methods used with a time of flight indicator on a homogeneous 65x65 fine grid. We have a thermal conductivity of 0.01, and a Péclet number of 6.2359. The injection well is in the lower left corner, while the production well is in the upper right corner.

As we can see in Figure 5.1, there are some slight differences in the position and shape in the coarse grid blocks, and in how the temperature is evolving, but the main aspects are the same. From Figure 5.2 we see that the temperature in the production well is higher for the fine grid than for the upscaled grids. This is because we have a larger coarse grid block than for the fine grid cell at the production well , so the cold water will reach the well faster for the upscaled grids because of the larger grid blocks. The accumulative errors are almost identical for the different refinement methods, there is a slightly lower error for the refineGreedy3 method. The amount of coarse grid blocks differ slightly, ranging from 94 to 109 grid blocks. The results of this test that there are not any large differences between the different refinement methods is as expected, because the different methods are quite similar to each other. We can however be lucky or unlucky every now and then that one refinement method will give us better or worse results than other methods. We have chosen to use refineGreedy2 in the following sections.

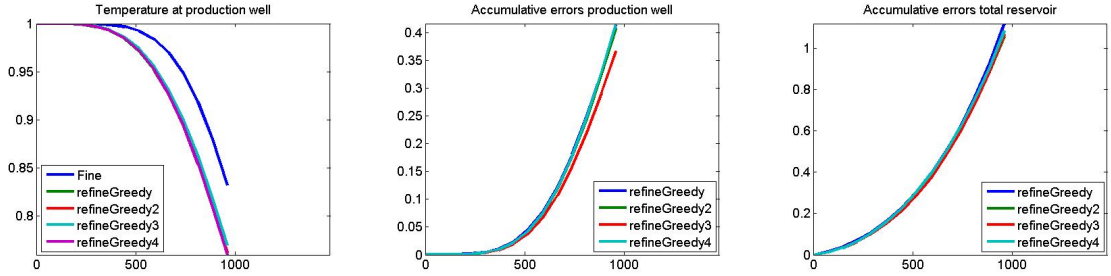

Figure 5.2: The temperature in the production well for different refinement methods after the simulation shown in Figure 5.1, and the accumulated relative errors compared to the fine scale grid for the production well and for the total reservoir. On the x-axis is time for all plots, and on the y-axis is the scaled temperature in plot one and the relative error in plot two and three.

5.2 Homogeneous medium

For our homogeneous medium we have a 65x65 celled fine grid. We will here explore the effect it has to add diffusion in the energy equation for increasing thermal conductivities. We first start with zero thermal conductivity, so the heat transport will be only convection. We then increase the thermal conductivity so the diffusion will eventually dominate the heat transport.

In our method we scale the temperatures and other variables, so 1 is the initial hot temperature of the reservoir, and 0 is the temperature of the injected cold water. We inject the cold water in the lower left corner, and pump up the warm water in the upper right corner. Since we are only interested in what happens when the thermal conductivity varies, we set the viscosity, density and permeability to 1, and the porosity to 0.35, and then we vary the thermal conductivity. We let our simulation run until we have 40 % remaining of the initial temperature.

We will look at grids that are upgridded based on Cartesian, permeability, velocity, and time of flight indicators, as we can see in Figure 5.3 and 5.4. We will compare the different accumulated relative errors of the temperature that the different upscaled grids has compared to the fine scale grid for the total reservoir and for the production well. Our first plot, Figure 5.3, has a thermal conductivity of $1 \cdot 10^{-2}$, and a Péclet number of 6.2359.

In Figure 5.3, we have convection dominated heat transport. We see that the different upscaled grids roughly has the same heat transport as the fine grid, but because the coarse grid blocks are larger, it reduces the resolution of the heat transport. We can also see on this figure that when we use the permeability indicator, we get an almost Cartesian grid, due to the permeability being homogeneous, while the flow based indicators and refinements produce a more non-Cartesian grid where it seems that the grid orientation is towards the production well. The production well temperature is constantly highest for the

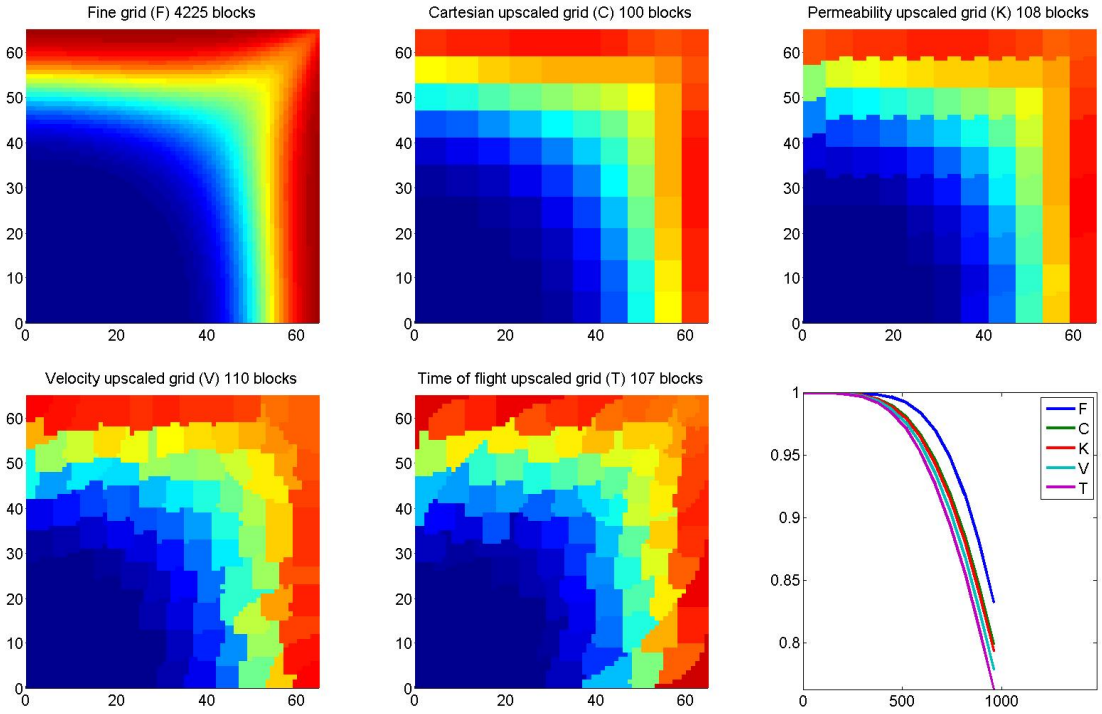

Figure 5.3: Simulations of temperature on a homogeneous 65x65 fine scale grid, and upscaled grids based on Cartesian, permeability, velocity, and time for flight indicators respectively. The thermal conductivity is $1 \cdot 10^{-2}$, and the Péclet number is 6.2359.

fine grid, followed by the Cartesian, permeability, velocity and time of flight based grids as we can see in the last plot in Figure 5.3. This might be because the heat transport in the flow based grids seems to go faster towards the production well than the more Cartesian grids.

We also do a simulation on the same grids but with a thermal conductivity of $5 \cdot 10^{-1}$, and Péclet number of 0.1247 as we can see in Figure 5.4.

Here in Figure 5.4, we see that the higher conductivity leads to a smearing of the temperature, so the front is more circular out from the injection well, and the temperature difference in the reservoir is smaller because the diffusion dominates the heat transport. In the convection dominated case in Figure 5.3, the front is more pointing towards to production well so the front looks more like a square, and the temperature is hot on the edges and cold from the injection well because we have very low diffusion, so the heat transport by flow is dominating. In Figure 5.4 we see that the temperature field looks roughly the same on each of the different grids but with lower resolution on the coarse grids. The temperature in the production well is quite equal as we see in the last plot in Figure 5.4 and also on the other plots by looking in the upper right corner. The diffusional smearing of the heat transport in the reservoir makes the temperature even out and reach equilibrium faster.

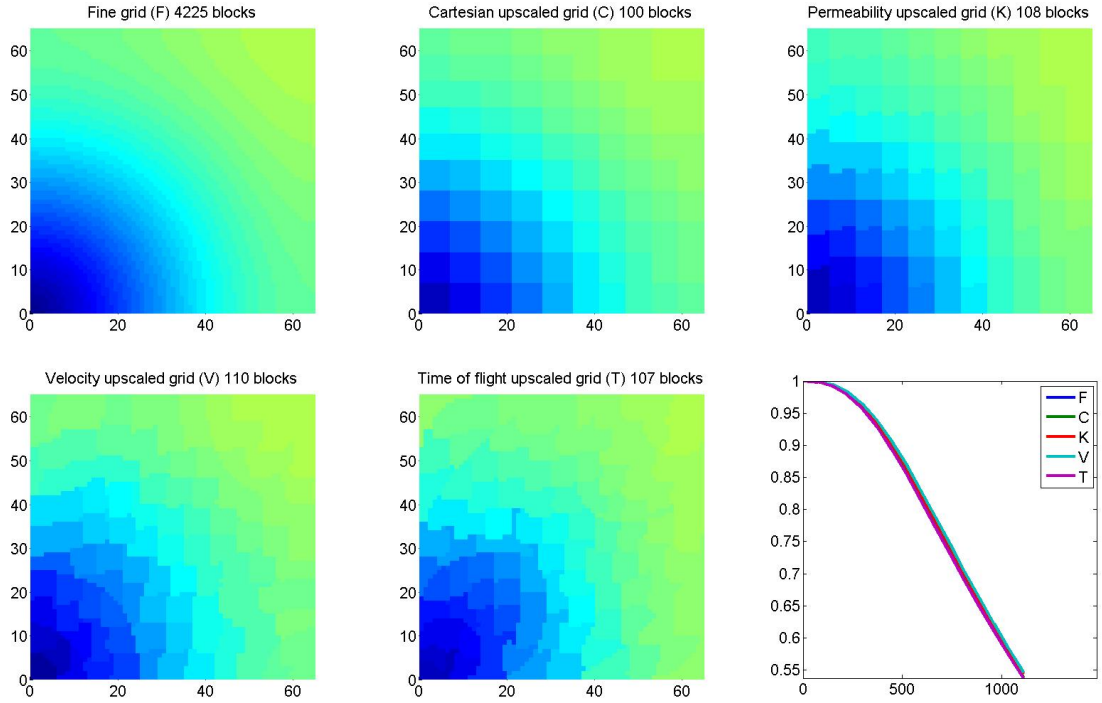

Figure 5.4: Fine scale grid and upscaled grids based on Cartesian, permeability, velocity, and time for flight indicators for a homogeneous 65x65 medium with thermal conductivity of $5 \cdot 10^{-1}$, and Péclet number of 0.1247. In the last plot we see the scaled temperature in the production well in the upper right corner over time. The injection well is in the lower left corner.

We run similar simulations to those in Figure 5.3 and 5.4 to find the accumulated relative errors for the production well and for the total reservoir for different thermal conductivities and Péclet numbers. We stop the simulations before the total temperature in the reservoir reach below 40 %. We first start the simulation with no thermal conductivity, which is what has been done before in [11] and [12]. We then increase the thermal conductivity until the diffusion is so large that it completely dominates, making the whole reservoir have the same temperature. The results of this we can see in Figure 5.5 and 5.6. When the Péclet number decrease, the diffusion increase.

Looking at figure 5.5 and 5.6, we notice that the flow-based coarse grids have the largest errors, especially for the convection dominated domain, while the Cartesian and permeability based grids have lower errors. The error decrease as the diffusion increase because the diffusion smears out the temperature, so the shape of the grid cells is less important, which leads to less errors.

In the total reservoir the Cartesian grid turns out to be the one with least error, and also its error at the production well is the lowest of the different grids when we have convection and diffusion dominated. In between convection dominated and diffusion dominated we

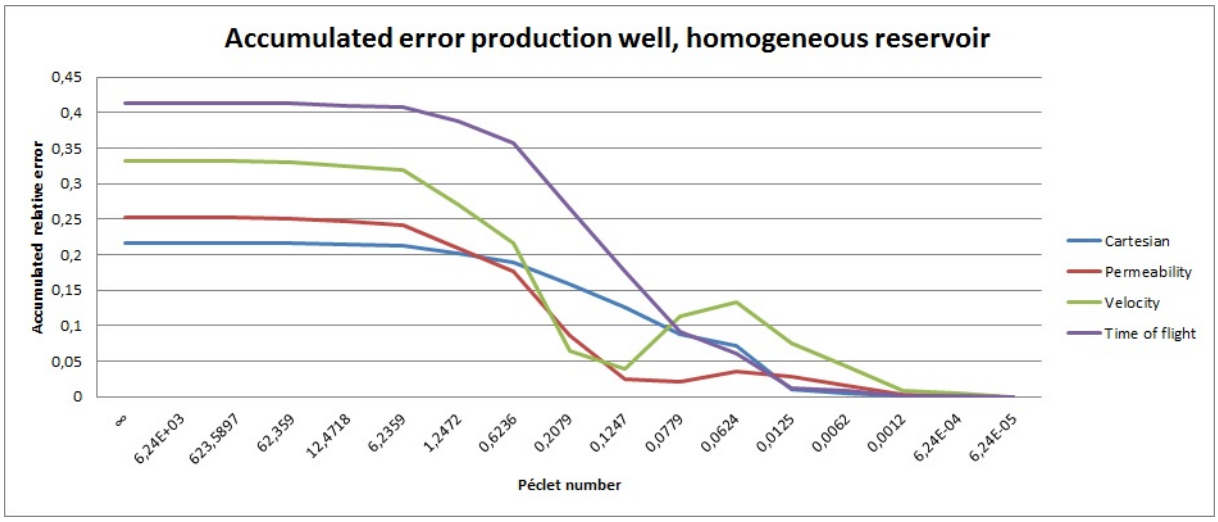

Figure 5.5: The accumulated relative error in the production well for a homogeneous medium. On the left side we have convection dominated, and on the right side we have diffusion dominated.

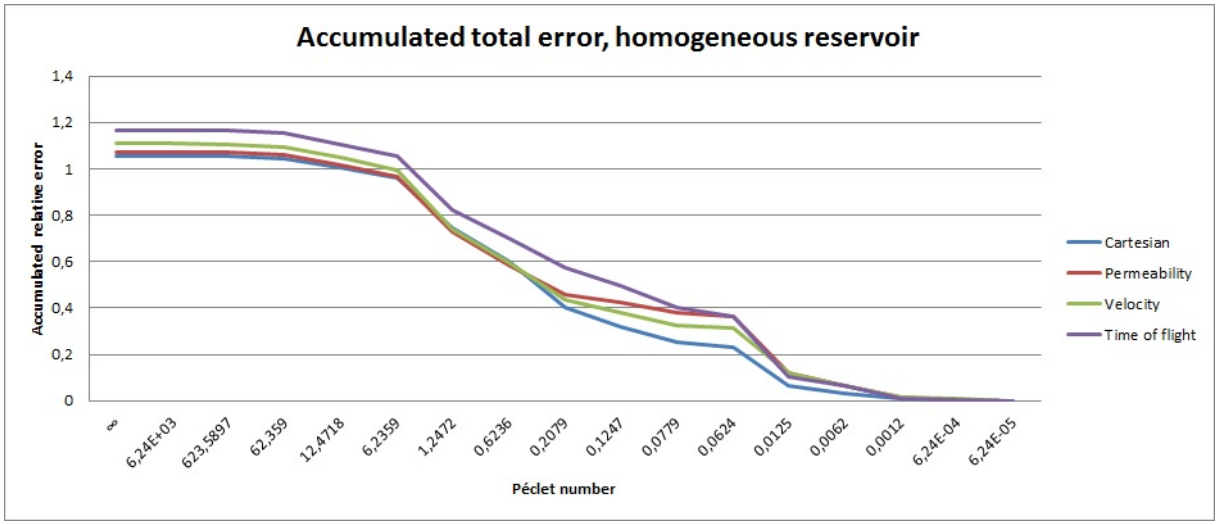

Figure 5.6: The accumulated relative error in the total reservoir for a homogeneous medium. On the left side we have convection dominated, and on the right side we have diffusion dominated.

have that the velocity and permeability based grids give lowest error at the production well. The errors can vary a bit with the upgrid input parameters when we create the grids.

5.3 Heterogeneous medium

For the heterogeneous medium we use SPE10, which is a comparative solution project which aims to compare different upgridding and upscaling approaches. SPE10 consists of 65 layers of 60x220 Cartesian grids. We will look at layer 25, which has a relatively smooth permeability. We will do the simulations in 2D. The results of the accumulated error in the production well and in the total reservoir can be seen in figure 5.10 and 5.11 respectively. We first start off with zero thermal conductivity, before we increase it, and by this decrease the dominance of the convection term. The Péclet number decrease when the diffusion increase.

For our first simulation, seen in Figure 5.7, we have zero thermal conductivity, and the Péclet number is infinite.

As we see from the different plots in Figure 5.7, the edges of the front is smeared out on the coarse grids due to the larger grid blocks, but the main features are preserved. This smearing makes some of the grid block temperatures seem a bit out of place compared to the fine grid. The temperatures at the production well is quite similar where Cartesian and permeability upscaled grids at start are more or less equal to the fine scale temperature, while the velocity and time of flight based upscaled grids have a slightly lower temperature at the production well compared to the fine scale grid.

We add thermal conductivity to our heat transport solver, and do another simulation. The result we can see in Figure 5.8 where we have $1{\cdot}10^{-7}$ thermal conductivity, corresponding to a Péclet number of $1 \cdot 10^6$. If we compare Figure 5.8 and Figure 5.7, we notice that the heat is smeared more out due to the higher diffusion. Because of this smearing the hot coarse grid blocks that were surrounded by colder grid blocks in Figure 5.7 are now smeared out in Figure 5.8, and the coarse grids looks better. The production well temperature is now more or less equal to the Cartesian and permeability upscaled grids the whole time.

We increase the thermal conductivity further to $1 \cdot 10^{-5}$, which gives a Péclet number of $1 \cdot 10^4$, and we run a heat transport simulation. The results we can see in Figure 5.9. We here see that the temperature is smeared out in the reservoir because of the high diffusion. The convection is not very important in this regime. From the plots we see that the Cartesian upscaled grid is most similar to the fine scale grid, followed by the velocity and time of flight upscaled grids. There seems to be something unusual going on with the permeability upscaled grid, that its heat does not diffuse as good as for the other grids. The flow based upscaled grids also have a bit warmer in the top of the reservoir compared to the fine scale grid and the Cartesian grid. The temperature at the production well is highest for the permeability upscaled grid, as we can also see in its plot. The velocity and time of flight temperatures at the production well are almost equal to each other, and these temperatures are slightly higher than for the fine scale grid and the Cartesian grid, which are more or less on top of each other in the plot for the temperature in the production well.

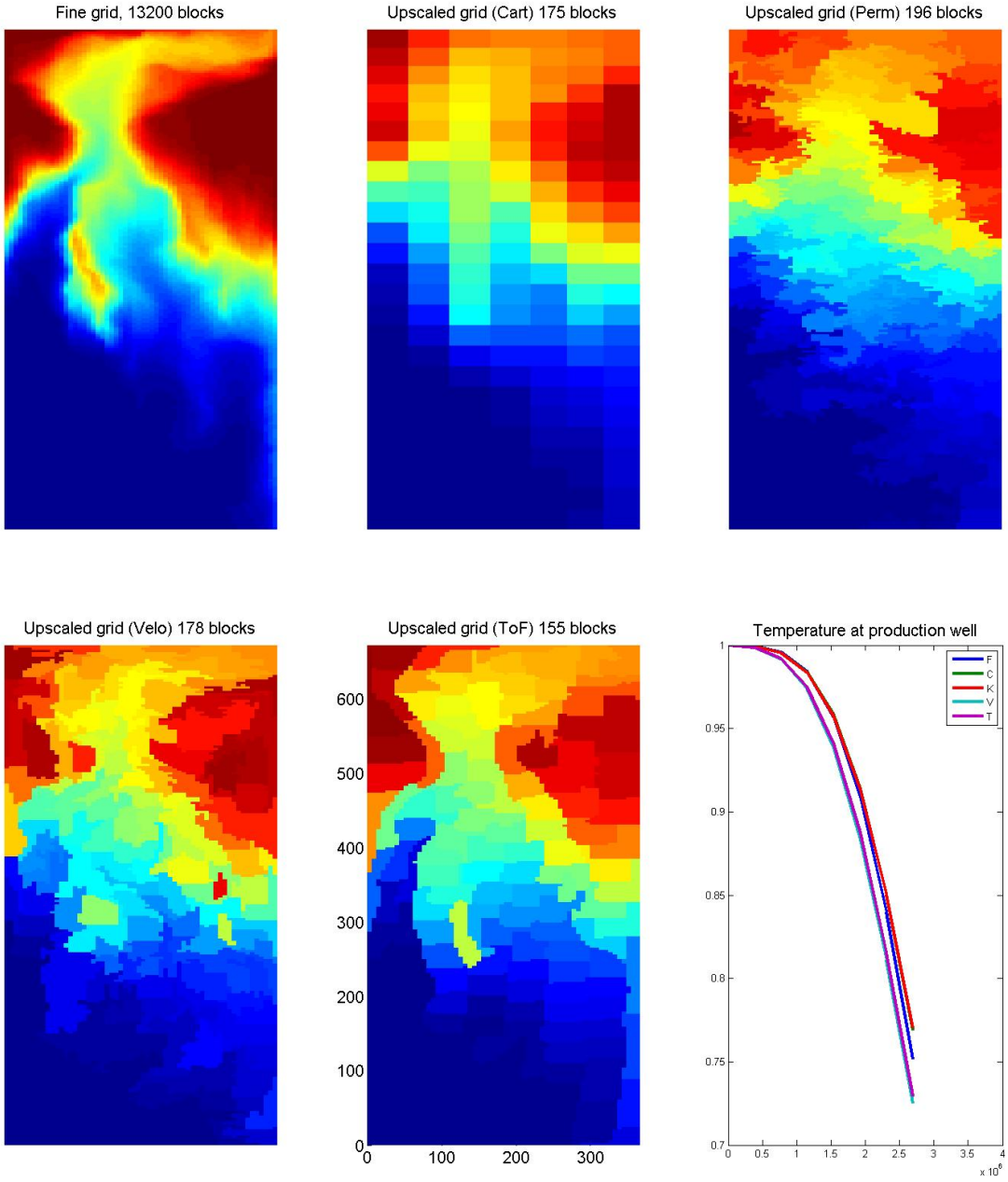

Figure 5.7: Simulations of temperature on a heterogeneous 60x220 fine scale grid, and upscaled grids based on Cartesian, permeability, velocity, and time for flight indicators respectively. The thermal conductivity is zero, and the Péclet number is infinite, so here we have only convection.

We do simulations for several more thermal conductivities and plot the results for the accumulated relative errors for the production well and for the total reservoir compared to

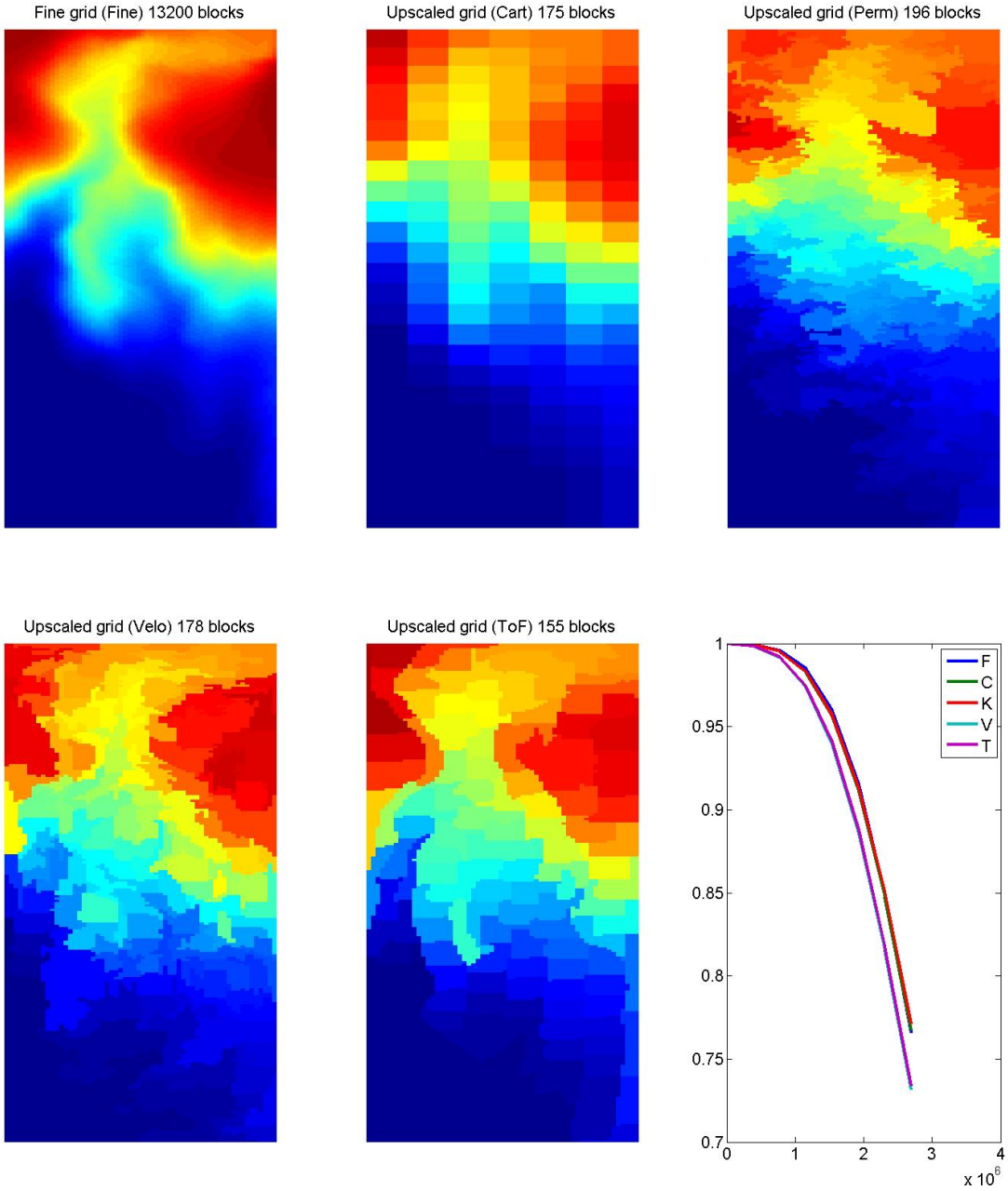

Figure 5.8: Simulations of temperature on a heterogeneous 60x220 fine scale grid, and upscaled grids based on Cartesian, permeability, velocity, and time for flight indicators respectively. The thermal conductivity is $1 \cdot 10^{-7}$, and the Péclet number is $1 \cdot 10^{6}$, so here we have mostly convection with a bit diffusion.

the fine scale grid. The results are plotted in Figure 5.10 and 5.11 respectively.

As we can see on Figure 5.10 and 5.11, the Cartesian grid has the lowest error most of

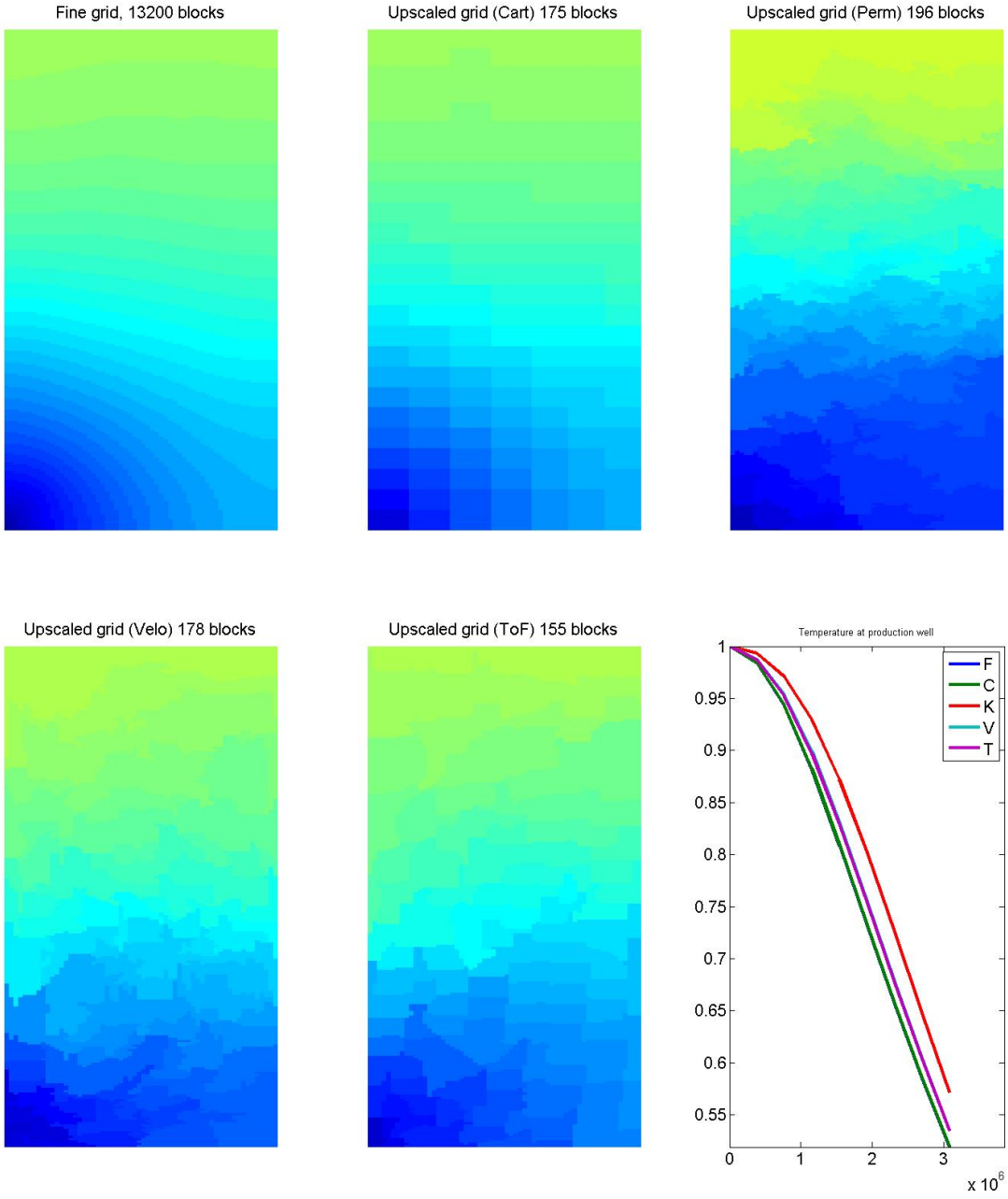

Figure 5.9: Simulations of temperature on a heterogeneous 60x220 fine scale grid, and upscaled grids based on Cartesian, permeability, velocity, and time for flight indicators respectively. The thermal conductivity is $1 \cdot 10^{-5}$, and the Péclet number is $1 \cdot 10^{4}$. The heat transfer on these plots are diffusion dominated.

the time. Velocity and time of flight based grids have medium error. The error in the total reservoir is decreasing when the diffusion increases because of the smearing of the

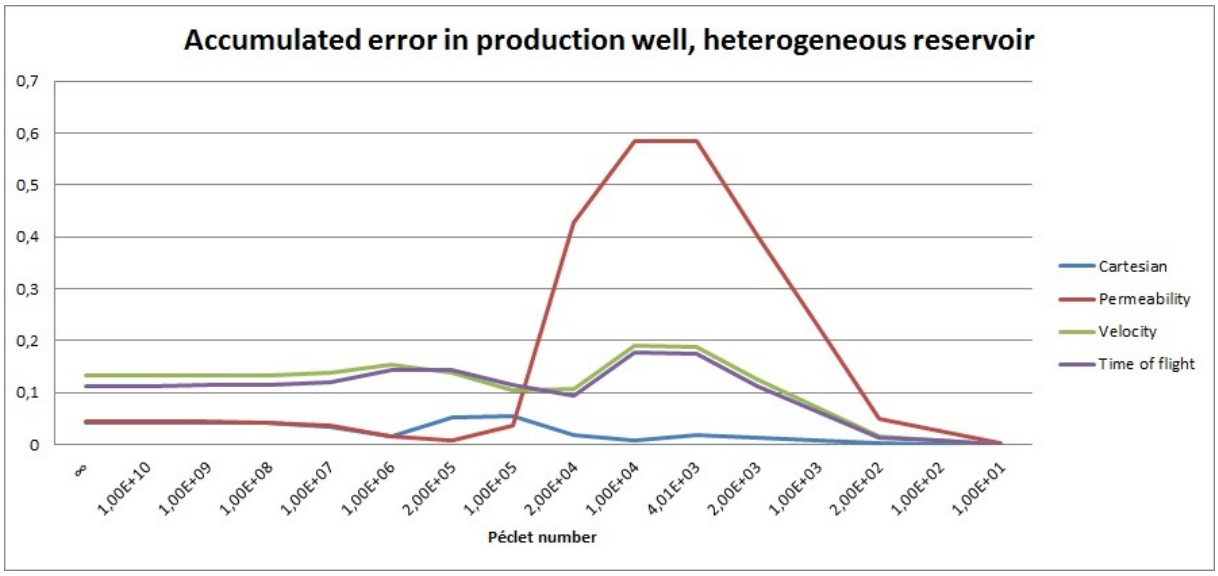

Figure 5.10: The accumulated relative error in the production well for a heterogeneous medium. On the left side we have convection dominated, and on the right side we have diffusion dominated.

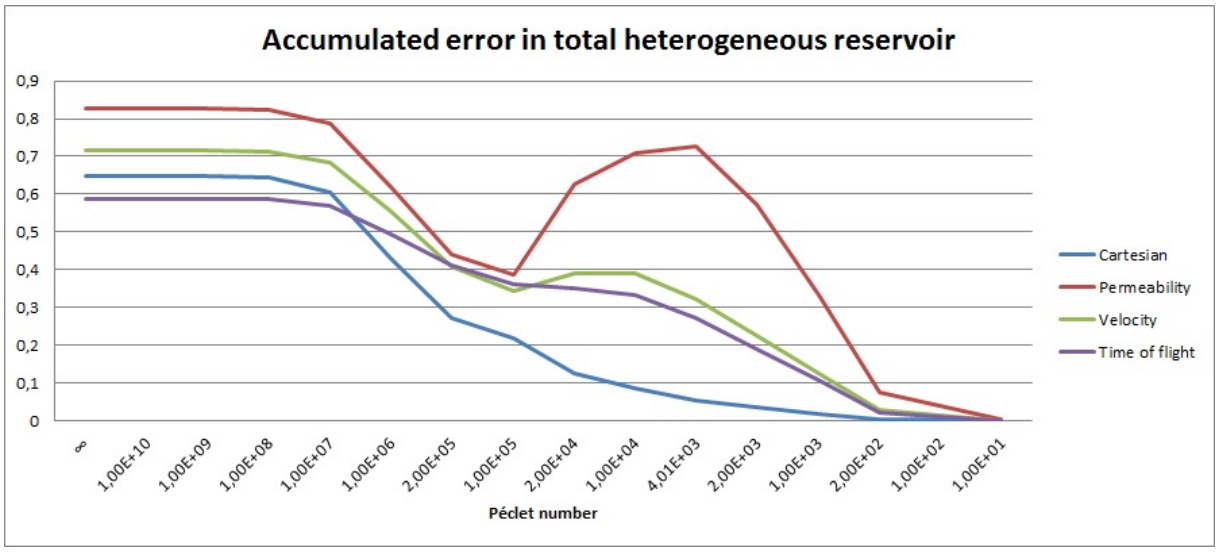

Figure 5.11: The accumulated relative error in the total reservoir for a heterogeneous medium. On the left side we have convection dominated, and on the right side we have diffusion dominated.

temperature, which makes it less important what the shapes of the coarse grid blocks are. This we also saw for the homogeneous case in the previous section. The permeability based upscaled grid has an unexpected big peak error of unknown cause for both the production well and for the total reservoir. We could also notice this by looking at Figure 5.9 that

there is something that seems a bit odd for the permeability upscaled grid. We do not know what cause this peak error, we tried looking through our simulation program, but we did not see anything that seemed wrong. From looking at Figure 5.9, it can seem like the diffusion dominated regime is not working as well for the indicator based upscaled grids as for the Cartesian grid, and especially not for the permeability upscaled grid. There is also a slightly higher error for the velocity and time of flight based grids in the diffusion dominated regime, but not as significant as for the permeability upscaled grids.

Because we have some freedom in choosing parameters for the merge and refine algorithms, we wanted to see if this could be the cause of the high peak in permeability accumulated error. For the grids we used in Figure 5.10 and 5.11, we set our lower volume bound to 30, and our upper flow bound to 80. To see if we got any different results we changed these bounds to 10 and 60 respectively, and ran a new simulation keeping all the other parameters equal. With the new bounds we get more grid cells for all the upscaled grids except for the Cartesian one which remains unaffected of this change. The new accumulated error results are shown in Figure 5.12 and 5.13.

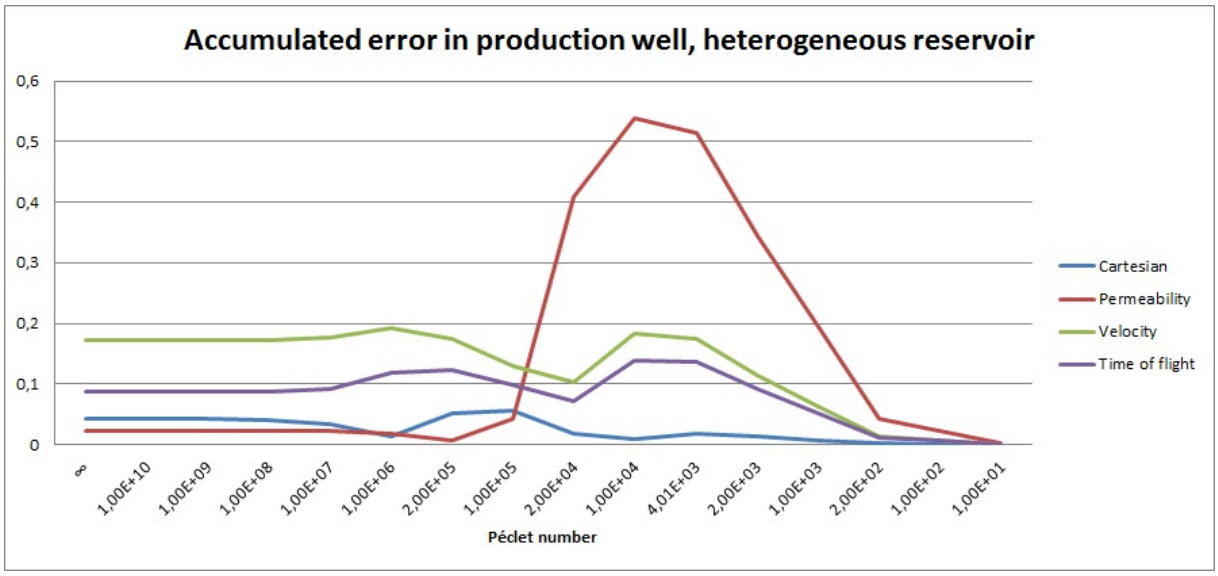

Figure 5.12: The accumulated relative error in the production well for a heterogeneous medium with more cells than 5.10. On the left side we have convection dominated, and on the right side we have diffusion dominated.

When comparing these new results with the previous results, we see that the permeability indicator based upscaled grid temperature errors remains more or less equal to the first simulation. We also notice that the difference between the velocity and time of flight indicator based upscaled grids temperature error has increased, while they previously had more similar errors. From this test we conclude that the change of refine and merge parameters will have some slight effect on the results, but the main features will be preserved.

In general from the results, we notice that the Cartesian grid gives the smallest error when

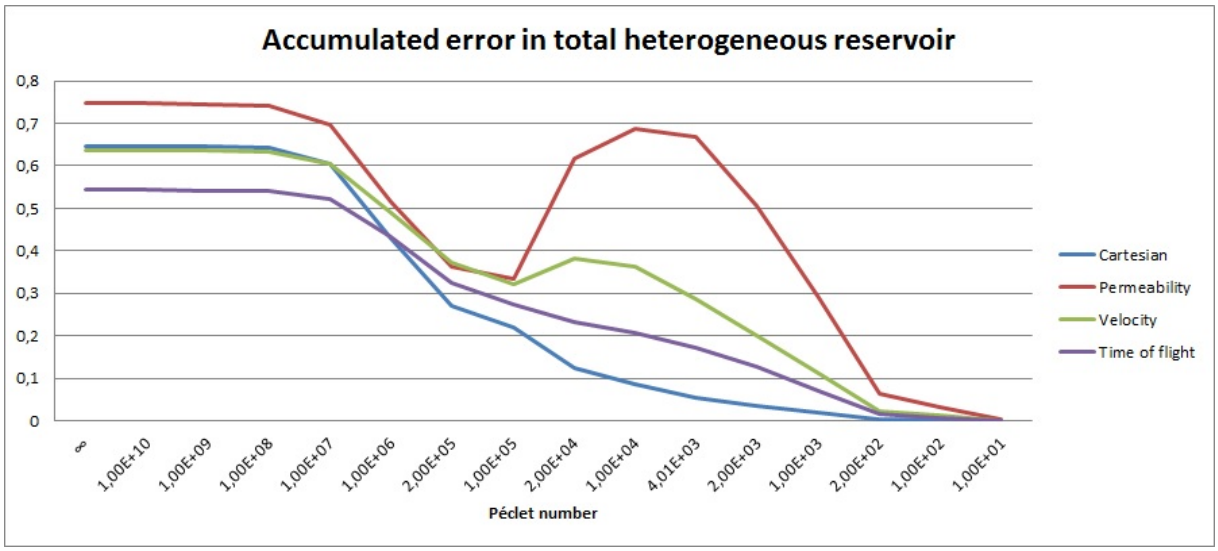

Figure 5.13: The accumulated relative error in the total reservoir for a heterogeneous medium with more cells than 5.11. On the left side we have convection dominated, and on the right side we have diffusion dominated.

the diffusion is dominating the reservoir. When convection is dominating, there may be grids that are better but overall the Cartesian grid should be a good choice of grid for this solver.

Chapter 6

Summary and further work

We have now upscaled and solved the energy equation for a homogeneous grid and for a heterogeneous grid with Cartesian, permeability, velocity and time of flight indicator based upscaling methods. From our results, we see that the different upscaling methods gives a bit different results in regards to error compared to the fine scale grid. It's hard to know which grid is better to choose before doing the simulations, but for most cases, and especially for heterogeneous media, it seems like the Cartesian upscaled grid did well. However it might not be the best option for all thermal conductivities and Péclet numbers, and other grids may have lower error. It was an unexpected peak error for the permeability indicator based upscaled grid when the diffusion dominates. We are not sure what may cause this larger error, but it may have something to do with the upscaling of the thermal conductivity, and the way we define the upscaled cell centers, face centers and face normals, but it is not certain this is the cause. This needs further testing to see if this is the cause of the error and how to reduce it.

According to previously done work by [11] and [12], the flow based upscaling should be better than the Cartesian grid for zero thermal conductivity. This is of course dependent on the grid structure and the input parameters when we make the grid, and it is hard to know what input parameters to use to get the lowest error, and which indicator to use a priori. In their work they also did simulation on injection of water into an oil reservoir. We solve a linear set of equations, while equations on oil and water reservoirs and non-linear. Future work could be to compare their work to the results we have gotten in this thesis, to see if there are similarities or if they are completely different for the same grids.

Our results for zero thermal conductivity is that Cartesian upscaled grid followed by permeability based upscaled grid had lowest error for a homogeneous reservoir 5.5, 5.6, while time of flight had the largest error and velocity had the second largest error. For the heterogeneous grid, time of flight based upscaled grid had the lowest error, followed by the Cartesian grid, while the permeability based upscaled grid had the largest error, and the velocity based grid had the second largest error for the total reservoir 5.11. In the

production well for a heterogeneous reservoir the permeability based upscaled grid had the lowest error, followed by the Cartesian upscaled grid 5.10. Velocity had the largest error, and time of flight had the second largest error.

Our results show that the implementation of diffusion into the energy equation, and upscaling of this equation works best on a Cartesian upscaled grid for the diffusion dominated regime when the reservoir is heterogeneous. This method on indicator based upscaled heterogeneous grids still needs some investigation for the diffusion dominated domain so we can find out what cause the increased errors and how to decrease it, especially for the permeability. It could also be interesting to compare this method to different methods in regards of errors and calculation time.

Hopefully the method we have presented here can be evolved and used in the future for simulating heat transport in geothermal reservoirs.

Bibliography

[1] R. Eymard, T. Galloiet, and R. Herbin. *Finite Volume Methods.* Handbook of Numerical Analysis, 7:713-1020, 2003.

[2] D.Kincaid and W. Cheney. *Numerical Analysis: Mathematics of Scientific Computing (Third Edition)* American Mathematical Society, 2002.

[3] International Energy Agency *Key World Energy STATISTICS 2013.* http://www.iea.org/publications/freepublications/publication/KeyWorld2013.pdf, February 2013.

[4] K.-A. Lie, S. Krogstad, I. S. Ligaarden, J. R. Natvig, H. M. Nilsen, and B. Skaflestad. *Open source MATLAB implementation of consistent discretisations on complex grids.* Computational Geosciences, 16(2):297-322, 2012.

[5] J. W. Tester, E. M. Drake, M. J. Driscoll, M. W. Golay, W. A. Peters *Sustainable Energy: Choosing Among Options.* Massachusetts Institute of Technology Press, 2005.

[6] J. M. Nordbotten and M. A. Celia. *Geological Storage of CO2: Modeling Approaches for Large-Scale Simulation.* John Wiley and Sons, 2012.

[7] D. A. Nield, A. Bejan. *Convection in Porous Media (4th edition).* Springer, 2013.

[8] T. H. Sandve. *Multiscale simulation of flow and heat transport in fractured geothermal reservoirs.* PhD Thesis, University in Bergen, 2013.

[9] V. Lampe. *Modelling Fluid Flow and Heat Transport in Fractured Porous Media.* Master Thesis, University in Bergen, 2013.

[10] V. L. Hauge. *Multiscale Methods and Flow-based Gridding for Flow and Transport in Porous Media.* PhD Thesis, Norwegian University of Science and Technology, 2010.

[11] J. E. Aarnes, V. L. Hauge, and Y. Efendiev. *Coarsening of Three-Dimensional Structured and Unstructured Grids for Subsurface Flow.* Advances in Water Resources, 30(11):2177–2193, 2007.

[12] V. L. Hauge, K-A. Lie, and J. R. Natvig.
Grid Coarsening Based On Amalgamation For Multi-Fidelity Transport Solvers.
Norwegian University of Science and Technology, 2010.

[13] BBC News. Turkey coal mine disaster: Desperate search at Soma pit. *http://www.bbc.com/news/world-europe-27408394.* June, 2014.

[14] Chinadaily. Coal mining: Most deadly job in China.
http://www.chinadaily.com.cn/english/doc/2004-11/13/content_391242.htm. June, 2014.